



FRM4SST-CRICR-NPL-003_ISSUE-1

Fiducial Reference Measurements for Sea Surface Temperature (FRM4SST)

D90 - Result from CEOS International Thermal Infrared Radiometer Inter-comparison (CRIC)

Part 3 of 3: Field Comparison of Radiometers

ESA Contract No. 4000127348/19/NL/IA

Yoshiro Yamada, NPL

Subrena Harris, NPL

Werenfrid Wimmer, Univ. of Southampton

Raymond Holmes, Univ. of Southampton

Tim Nightingale, STFC Rutherford Appleton Laboratory

Arrow Lee, STFC Rutherford Appleton Laboratory

Nis Jepsen, Danish Meteorological Institute

Nicole Morgan, CSIRO / Australian Bureau of Meteorology

Frank-M. Göttsche, Karlsruhe Institute of Technology

Raquel Niclòs, Univ. of Valencia

Martín Perelló, Univ. of Valencia

Vicente Garcia-Santos, Univ. of Valencia

Craig Donlon, European Space Agency

Nigel Fox, NPL

March 2022

INTENTIONALLY BLANK

Fiducial Reference Measurements for Sea Surface Temperature (FRM4SST)

D90 – Results from CEOS International Thermal Infrared Radiometer
Inter-comparison (CRIC)
Part 3 of 3: Field Comparison of Radiometers

Yoshiro Yamada, Subrena Harris, Werenfrid Wimmer, Raymond Holmes,
Tim Nightingale, Arrow Lee, Nis Jepsen, Nicole Morgan, Frank-M.
Göttsche, Raquel Niclòs, Martín Perelló, Vicente Garcia-Santos, Craig
Donlon & Nigel Fox

© NPL Management Limited, 2022

National Physical Laboratory
Hampton Road, Teddington, Middlesex, TW11 0LW

Extracts from this report may be reproduced provided the source is acknowledged
and the extract is not taken out of context.

Approved on behalf of NPLML by
Martin Dury, Science Area Leader.

DOCUMENT MANAGEMENT

Issue	Revision	Date of Issue/revision	Description of Changes
1	1	19/12/2022	Creation of document (Draft A)
	2	30/03/2023	Draft B

DOCUMENT APPROVAL
Contractor Approval

Name	Role in Project	Signature & Date (dd/mm/yyyy)	
Y Yamada	Metrology lead and comparison pilot	<i>G.Y.</i>	30/03/2023
N Fox	Metrology lead and CEOS WGCV rep	<i>Nigel Fox</i>	30/03/2023

CUSTOMER APPROVAL

Name	Role in Project	Signature	Date (dd/mm/yyyy)
C Donlon	ESA Technical Officer		

APPLICABLE DOCUMENTS

AD Ref.	Ver. /Iss.	Title
AD-1	Issue – 1	Fiducial Reference Measurements for Sea Surface Temperature (FRM4SST): Protocol for FRM4SST CRIC Laboratory Comparison of Radiometers and Blackbodies
AD-2	Issue – 1	Fiducial Reference Measurements for Sea Surface Temperature (FRM4SST): Protocol for FRM4SST CRIC Field Comparison of Radiometers
AD-3	Issue – 2	Fiducial Reference Measurements for Sea Surface Temperature (FRM4SST): D80 - Implementation plan for Laboratory and Field Comparisons of Radiometers and Blackbodies
AD-4	Issue – 1	Fiducial Reference Measurements for Sea Surface Temperature (FRM4SST): D90 – Results from CEOS International Thermal Infrared Radiometer Inter-comparison (CRIC) Part 1 of 3: Laboratory Comparison of Blackbodies
AD-5	Issue – 1	Fiducial Reference Measurements for Sea Surface Temperature (FRM4SST): D90 – Results from CEOS International Thermal Infrared Radiometer Inter-comparison (CRIC) Part 2 of 3: Laboratory Comparison of Radiometers

CONTENTS

1	INTRODUCTION	1
2	ORGANISATION OF THE COMPARISON	2
2.1	PILOT.....	2
2.2	PARTICIPANTS	2
3	TIMELINE	2
4	COMPARISON SCHEME	3
4.1	VENUE.....	3
4.2	INSTALLATION OF THE RADIOMETERS.....	4
5	PARTICIPANTS' RADIOMETERS AND MEASUREMENTS	6
5.1	MEASUREMENT BY UOV	7
5.1.1	Description of radiometer, route of traceability and uncertainty contributions	7
5.1.2	Measured data	11
5.2	MEASUREMENT BY KIT	12
5.2.1	Description of radiometers, route of traceability and uncertainty contributions... ..	12
5.2.2	Measured data	14
5.3	MEASUREMENT BY CSIRO	16
5.3.1	Description of radiometer, route of traceability and uncertainty contributions	16
5.3.2	Measured data	17
5.4	MEASUREMENT BY RAL.....	19
5.4.1	Description of radiometer, route of traceability and uncertainty contributions	19
5.4.2	Description of radiometer, route of traceability and uncertainty contributions	19
5.4.3	Measured data	19
5.5	MEASUREMENT BY UOS	20
5.5.1	Description of radiometer, route of traceability and uncertainty contributions	20
5.5.2	Measured data	22
5.6	MEASUREMENT BY DMI	24
5.6.1	Description of radiometer, route of traceability and uncertainty contributions	24
5.6.2	Measured data	25
6	COMPARISON RESULT	27
7	DISCUSSIONS	32
8	CONCLUSIONS	35
	REFERENCES	35

ACRONYMS AND ABBREVIATIONS

CEOS	Committee on Earth Observation Satellites
IR	Infra-Red
NPL	National Physical Laboratory
SST	Sea Surface Temperature
WGCV	Working Group for Calibration and Validation
RSS	Root Sum Square
PRT	Platinum Resistance Thermometer
BB	Blackbody

1 INTRODUCTION

The measurement of the Earth's surface temperature is a critical product for meteorology and an essential parameter/indicator for climate monitoring. Satellites have been monitoring global surface temperature for some time, and have established sufficient consistency and accuracy between in-flight sensors to claim that the measurement is of "climate quality". However, it is essential that such measurements are fully anchored to International System of Units (SI) and that there is a direct regular correlation with "true" surface/in-situ based measurements.

The most accurate of these surface-based measurements (used for validation) are derived from field-deployed IR radiometers. These are in principle calibrated traceably to SI, generally through a reference radiance blackbody (BB). Such instrumentation is of varying design, operated by different teams in different parts of the globe. It is essential for the integrity of their use, to provide validation data for satellites in-flight and to provide the link to future sensors, that any differences in the results obtained between them are understood. This knowledge will allow any potential biases to be removed and not transferred to satellite sensors. This knowledge can only be determined through formal comparison of the instrumentation, both in terms of its measurement capabilities in relation to primary "laboratory based" calibration facilities, and its use in the field. The provision of a fully traceable link to SI as part of this process ensures that the data are evidentially robust and can claim their status as a "climate data record".

The "satellite IR Cal/Val community" is well versed in the need and value of such comparisons having held highly successful exercises in Miami in 2001 [1, 2], and at the National Physical Laboratory (NPL), Teddington UK, in 2009 [3, 4] and in 2016 [5, 6, 7, 8], all carried out under the auspices of CEOS. However, six years had passed since the last comparison and it was considered timely to repeat/update the process, and so a similar comparison was repeated in 2022. The 2022 comparison included:

- a. Comparison of the BB reference standards used for calibrating the radiometers (laboratory based).
- b. Comparison of the radiometer response to a common SI-traceable BB target (laboratory based).
- c. Evaluation of differences in radiometer response when viewing Sea surface targets in particular the effects of external environmental conditions such as sky brightness (field based).

The comparison took place during two weeks in June of 2022. The first week involved the laboratory-based comparisons (a. b.) at NPL. The second week was devoted to the field-based comparison (c.), at the tip of Boscombe Pier in Bournemouth, UK. Unlike the previous comparison in 2016, land surface temperature measurement was not a part of the 2022 comparison. Details of all the comparisons including comparison scheme can be found in the protocols of the comparisons [AD-1, AD-2] and the implementation plan [AD-3].

This is Part 3 of a three-part report, and covers the result of the field comparison of the radiometers of the participants at Boscombe Pier. Reports on the laboratory comparisons held at the NPL can be found in Parts 1 and 2 [AD-4, AD-5].

2 ORGANISATION OF THE COMPARISON

2.1 PILOT

As in the recent previous comparisons, NPL, the UK national metrology institute (NMI), served as pilot for the 2022 comparison. NPL, as the pilot, was responsible for inviting participants, for preparing the protocols that the participants have agreed, for providing the implementation plan to enable participants to prepare for the comparison, for the analysis of data following appropriate processing by individual participants and for the compilation of a report that is agreed by all participants.

The selection and arrangement of the seaside venue was made with the support of the University of Southampton (UoS). It should be noted that NPL did not take part in the field-based sea surface temperature (SST) measurement itself, and only assumed the role of the coordinating pilot.

2.2 PARTICIPANTS

A call was made inviting potential participants in the related scientific community to express their interest to participate in December 2021. The list of participants that actually participated is shown in Table 1. As can be seen, seven participants including the pilot took part. This is a reduction from the previous 2016 comparison where eleven institutes, including the pilot, were present. Although there was a certain number of expressed interests, no institute could participate from the USA and China, primarily due to travel restrictions imposed due to the COVID-19 pandemic.

Table 1. Comparison participants

Contact person	Short version	Institute
Yoshiro Yamada (pilot)	NPL	National Physical Laboratory Hampton Road, Teddington, Middlesex, TW11 0LW, United Kingdom
Werenfrid Wimmer	UoS	University of Southampton, European Way, Southampton, SO19 9TX, United Kingdom
Tim Nightingale	RAL	STFC Rutherford Appleton Laboratory Harwell Campus, Didcot, Oxon OX11 0QX, United Kingdom
Nis Jepsen	DMI	Danish Meteorological Institute, Lyngbyvej 100, 2100 Copenhagen Ø, Denmark
Nicole Morgan	CSIRO	CSIRO / Australian Bureau of Meteorology CSIRO, 3-4 Castray Esplanade, Battery Point, TAS 7150 Australia
Frank-M. Götsche	KIT	IMK-ASF / Karlsruhe Institute of Technology, Hermann-von-Helmholtz-Platz 1, 76344 Eggenstein-Leopoldshafen, Germany
Raquel Niclòs	UoV	Dept. of Earth Physics and Thermodynamics, University of Valencia. 50 Dr. Moliner. ES-46100, Burjassot (Valencia), Spain

3 TIMELINE

The preparation for the comparison, the comparison measurements, and the analysis and report writing were conducted according to the timeline shown in Table 2. The seaside comparison was undertaken in the week 20 – 24 June 2022, following the week of laboratory comparison at the NPL.

Table 2. Comparison activity timeline

Invitation to participate	December 2021
Formal agreement of protocol	May 2022
Participants send preliminary report of measurement system and uncertainty to pilot	May 2022
Laboratory measurement of participants' radiometers against reference blackbodies. Laboratory measurement of participants' blackbodies by reference thermometer.	13 – 17 June 2022

SST measurement comparison of participants' radiometers.	20 – 24 June 2022
Participants send all data and reports to pilot	~ August 2022
Pre-Draft A result communication with individual participants for comments, corrections and confirmation	~ November 2022
Draft A report circulation among participants (tentative)	December 2022
Draft B report submission to CEOS WG (tentative)	March 2023

4 COMPARISON SCHEME

4.1 VENUE

The field comparison was conducted at the Boscombe Pier in Bournemouth, on the south coast of the United Kingdom. The location of the pier is shown in Fig. 1. The pier is located in the centre of a few kilometers' stretch of sandy beach, and extends southwards to the sea that connects to the English Channel. At the tip of the pier, a corner was fenced off so that the radiometers, data acquisition systems and other additional instruments could be placed. A generator was placed on-site to supply the necessary electricity. The pier is a public space, a local's favourite place for fishing. Therefore, the participants took turns to man the comparison site during the time the pier was accessible to the public to avoid any unlikely but unwanted interference. A photograph of the pier viewed from the land is shown in Fig. 2.

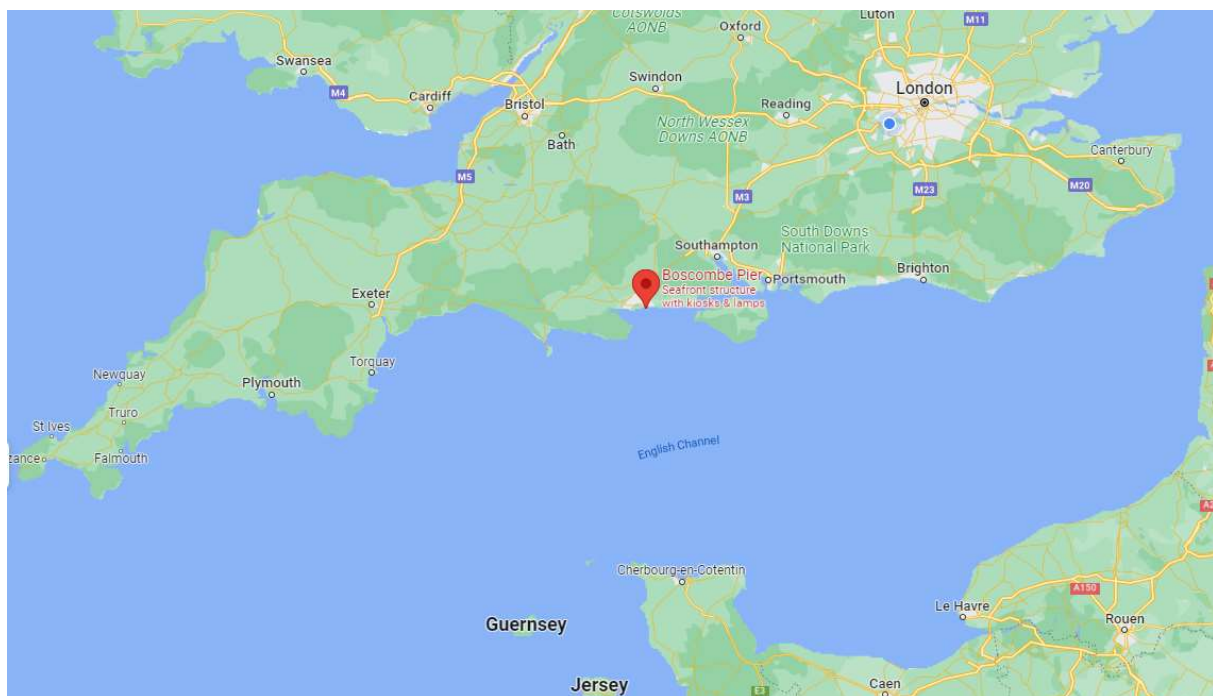


Figure 1 Location of Boscombe Pier, Bournemouth, UK (source: Google maps)



Figure 2 View of Boscombe Pier. The neighbouring Bournemouth Pier is also visible in the distance

4.2 INSTALLATION OF THE RADIOMETERS

The field comparison exercise was conducted by having the participants' radiometers simultaneously measure the SST. The participant radiometers were mounted on the platform outside the railing at the end of a seaside pier extending to the sea, viewing approximately the same area of the sea surface side by side. Care was taken by each participant to avoid the anti-fall wires from obstructing the radiometer field of view. Figure 3 shows the participants installing the radiometers by their individual methods in preparation for the measurement.



Figure 3 Radiometers being installed for measurement of the sea at the tip of the pier

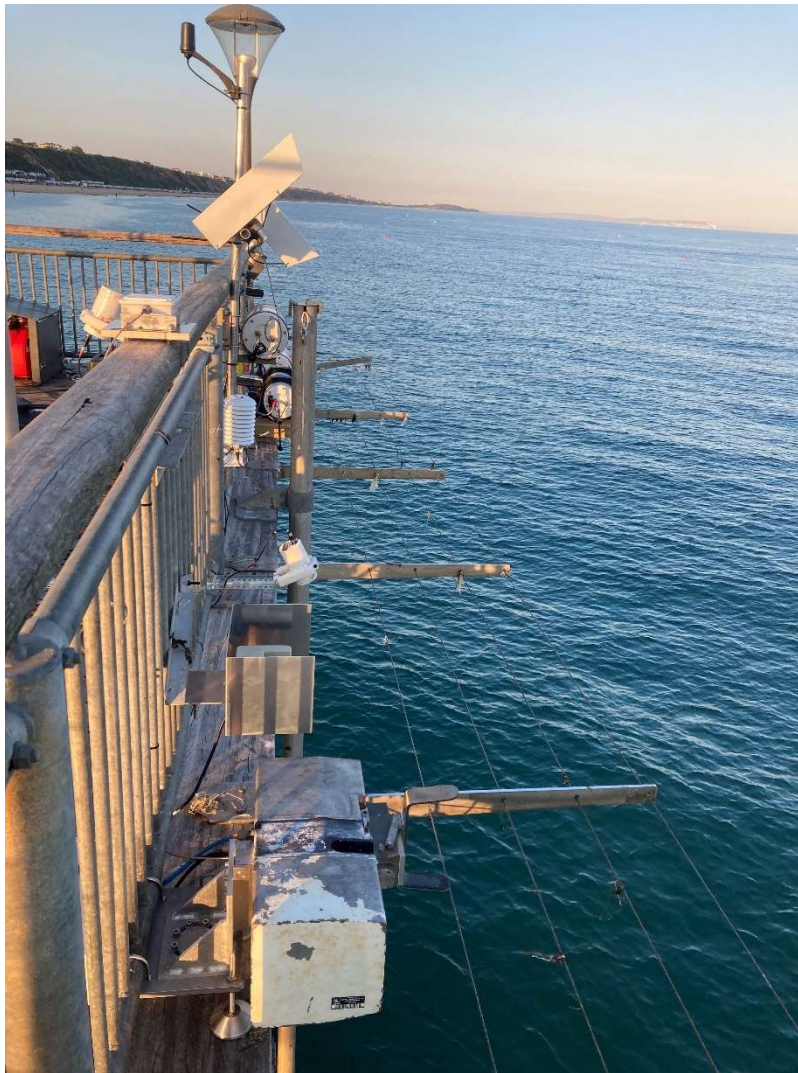


Figure 4 Radiometers viewing the sea surface.

The six radiometers after installation are seen in Fig. 4. RAL's large rectangular the Scanning Infrared Sea Surface Temperature Radiometer (SISTeR) is seen in the foreground. UoV's two cylindrical-shaped CIMEL radiometers are placed next (one down below viewing the sea, the other inside the railing viewing the sky), then KIT's two Heitronics radiometers with their distinctive long hoods are seen attached to a tall pole. Finally three large drum-shaped Infrared Sea surface temperature Autonomous Radiometer (ISAR) radiometers belonging to DMI, CSIRO and UoS, respectively, are visible towards the far end.

Most instruments had means of preventing rain contamination: SISTeR and ISARs had rain detectors which triggered covering of the detecting ports, while KIT radiometer were installed in protective housing with an extended viewing port cover, so the measurements were made continuously throughout the period (except for the UoV radiometer that was taken off each evening to avoid contamination from possible rainfall) and a comparison was made of the measurements made at the same time.

5 PARTICIPANTS' RADIOMETERS AND MEASUREMENTS

In the following, descriptions of the participants' radiometers are given, as reported by each participant, and measured data are shown for each participant. All date and time values are given in Coordinated Universal Time (UTC).

Each participant made measurements at different timings and intervals, and reported the SST and its associated standard uncertainty as described below. From this, the mean SST over 20 minute intervals as well as the mean standard uncertainty for the same intervals were evaluated for each participant. This was used to evaluate the agreement among participants in the next section.

5.1 MEASUREMENT BY UoV

5.1.1 Description of radiometer, route of traceability and uncertainty contributions

Make and type of the Radiometer: CIMEL Electronique CE312-2, six spectral bands (two units)

Outline Technical description of instrument: Type of detector: thermopile, operating at ambient temperature. Six spectral bands: B1 8.0 μm -13.3 μm , B2 10.9 μm -11.7 μm , B3 10.2 μm -11.0 μm , B4 9.0 μm -9.3 μm , B5 8.5 μm -8.9 μm , and B6 8.3 μm -8.6 μm . Broad band: germanium window and zinc sulphide filters. Narrow bands: interference filters. Field of view: 10°. The instrument has a built-in radiance reference made of a concealable gold-coated mirror which enables comparison between the target radiance and the reference radiation from inside the detector cavity. The temperature of the detector is measured with a calibrated platinum resistance thermometer (PRT), thus allowing compensation for the cavity radiation. The relevant outputs of the radiometer are the detector temperature and the difference in digital counts between the signals from the target and the detector cavity. For detail see [9, 10, 11].

Establishment or traceability route for primary calibration including date of last realisation and breakdown of uncertainty: The following error analysis is based on laboratory measurements with the Landcal BB P80P (total uncertainty of 0.34 K; [AD-4, AD-5]) on May, 2022, and estimates from the above references. BB measurements were taken at eleven fixed temperatures (from 0 °C to 50 °C) in two different runs with instrument realigning. The values reported below are typical values for all BB temperatures considered for **band 3** of each radiometer (units 1 and 2).

Uncertainty contributions:

As explained in the methodology section, the CE312-2 band 3 (10.2-11.0 μm) was selected for the field SST comparison.

Several parameters were varied for the uncertainty analysis, with the following ranges:

- A. Water surface temperatures from 290 to 293 K.
- B. Sky temperatures from 208 to 278 K.
- C. Wind speeds from 0 m/s to 15 m/s.
- D. Zenith angle from 22.5° to 27.5°.

These values are representative of the measurement conditions during the field SST comparison.

Type A

- Repeatability: Typical value of the standard deviation of 15 measurements at fixed black body temperature without re-alignment of radiometer.

Unit 1	B3
K	0.04
% (at 300 K)	0.014

Unit 2	B3
---------------	-----------

K	0.03
% (at 300 K)	0.009

- Reproducibility: Typical value of difference between two runs of radiometer measurements at the same black body temperature including re-alignment.

Unit 1	B3
K	0.05
% (at 300 K)	0.018

Unit 2	B3
K	0.04
% (at 300 K)	0.012

Total Type A uncertainty (RSS):

Unit 1	B3
K	0.07
% (at 300 K)	0.02

Unit 2	B3
K	0.05
% (at 300 K)	0.015

Type B

- Primary calibration: 0.34 K (estimation of the total uncertainty of the Landcal blackbody P80P).

- Water emissivity: 0.15 K. Emissivity values were computed following the methodology proposed by Niclos et al. in [12] based on the model of Wu and Smith [13] for sea surface. Water salinity does not affect the water surface emission and its angular variation in the region from 8 to 13 μm [14, 15], with negligible differences between fresh and sea water emissivities, mainly for the CE312 band 3 spectral range. Spectral values were integrated for the radiometer band (using the response function provided by the manufacturer) to obtain the band emissivity against wind speed and observation angle. A water emissivity uncertainty of 0.004 was considered for the analysis [16, 17]. Downwelling sky radiances were directly measured by the CE312-2 Unit 1 (band 3). The radiometer total uncertainty of 0.37 K could be considered for this term. In this case the water-emissivity associated uncertainty would be of 0.11 K. However, an uncertainty of 30% in the downwelling sky radiance was used for the analysis, due to the partially cloudy and variable sky conditions in different periods of the campaign (marked as “**clearly cloud-affected data**” in the dataset). **Although the downwelling sky radiance effect is relatively small, these sky conditions were not optimum for the SST comparison. We usually use cloud-free sky conditions for CAL/VAL activities.**

- Water surface “roughness”: 0.005 K. This term is related with wind speed. Surface wind produces roughness on the water surface, which can be characterized using an approximately normal and isotropic facet slope distribution. Wu and Smith considered this facet slope distribution to model the sea surface emissivity under several wind speed conditions, by taking into account also the effect of multiple surface reflections [13]. A wind speed uncertainty of 5 m/s was considered for the analysis. The wind speed effect is really low at a zenith angle of 25°.

- Angle of view to nadir: 0.005 K. A zenith angle uncertainty of 2.5° was considered for the analysis, even though we used a digital inclinometer (with a sensitivity of 0.1°) to set up the radiometers.

- Linearity of radiometer: 0.06 K (Typical value for all bands in the temperature range 0-40 °C according to [10]).

- Drift since calibration: 0.06 K. It has been corrected for using the calibration measurements performed with the Landcal blackbody P80P mentioned above. A linear correcting equation

has been derived for each band and radiometer, with the radiometer measured temperature and the detector temperature as inputs. The uncertainty for this correction is the RSS of the typical estimation uncertainty of the linear regression (0.06 K for unit 1 and 0.05 K for unit 2) and the uncertainties resulting from the propagation of input temperature errors (standard deviations for 15 measurement at a fixed temperature) in the linear correcting equation. The resulting uncertainty in the correction of calibration drift is 0.08 K for unit 1 and 0.06 K for unit 2.

Ambient temperature fluctuations: 0.04 K. The effect of ambient temperature fluctuations is compensated by the CE312 radiometers by measuring the detector cavity temperature by means of a calibrated PRT. The uncertainty in this process is the uncertainty of the internal PRT, which is 0.04 K according to [10].

Atmospheric absorption/emission: < 0.03 K. A vertical distance of 4 m can be considered between the radiometer and the water surface. For this short distance and the viewing angle of 25°, the atmospheric absorption is considered negligible [18].

Type A + Type B standard uncertainty (RSS): **0.39 K** (0.37 K for cloud-free data, with the emissivity associated uncertainty is 0.11 K, as mentioned before).

Table 3 Uncertainty contributions associated with the SST measurements in the field

Uncertainty Contribution	Type A Uncertainty in Value / K / %	Type B Uncertainty in Value / K (uncertainty source)	Standard uncertainty in Value / K
Repeatability of measurement	0.03 K / 0.009 %		0.03
Reproducibility of measurement	0.04 K / 0.012 %		0.04
Primary calibration		0.34	0.34
Water emissivity		0.15 (0.004 in emissivity, 30% in sky radiance (CE 312 unit 1, band 3))	0.15
Water surface "roughness"		0.005 (5 m/s in wind speed)	0.005
Angle of view to nadir		0.005 (2.5° in viewing angle)	0.005
Linearity of radiometer		0.06	0.06
Drift since last calibration		0.05	0.05
Ambient temperature fluctuations		0.04	0.04

Atmospheric absorption/emission		< 0.03	< 0.03
RSS total	0.05 K / 0.015 %		0.39*

***In cloud-free conditions, the combined standard uncertainty (RSS) is 0.37 K since the uncertainty contribution associated to water emissivity can be considered of 0.11 K, instead of 0.15 K.**

IMPORTANT NOTE: In some periods the CE312-2 Unit 1, which measured the downwelling sky radiance at 25° (from Zenith), was unfortunately pointing to the sun (with solar zenith and azimuth angles within the radiometer field of view), and the measured sky radiances were abnormally high. Data corresponding to these periods have been removed from the dataset due to this anomaly. These periods were: 20 June 2022: 11:31:59 - 12:13:09; 21 June 2022: 11:29:31 - 12:09:43; and 22 June 2022: 11:23:37 - 12:03:08, in UTC time.

Operational methodology during measurement campaign: specular reflection is approximated for the sea surface reflection. This is the usual approximation for the water surface (Barton et al., 1989) without foam coverage (Nicolòs et al. 2007). The reflection term can be rewritten as:

$$L_i^{ref}(\theta, \phi) = [1 - \varepsilon_i(\theta, \phi)]L_{i\ atm}^{\downarrow}(\theta, \phi \pm \pi)$$

and the radiometer observing the water surface at a direction (θ, ϕ) measures:

$$L_i(\theta, \phi) = \varepsilon_i(\theta, \phi)B_i(T) + L_i^{ref}(\theta, \phi)$$

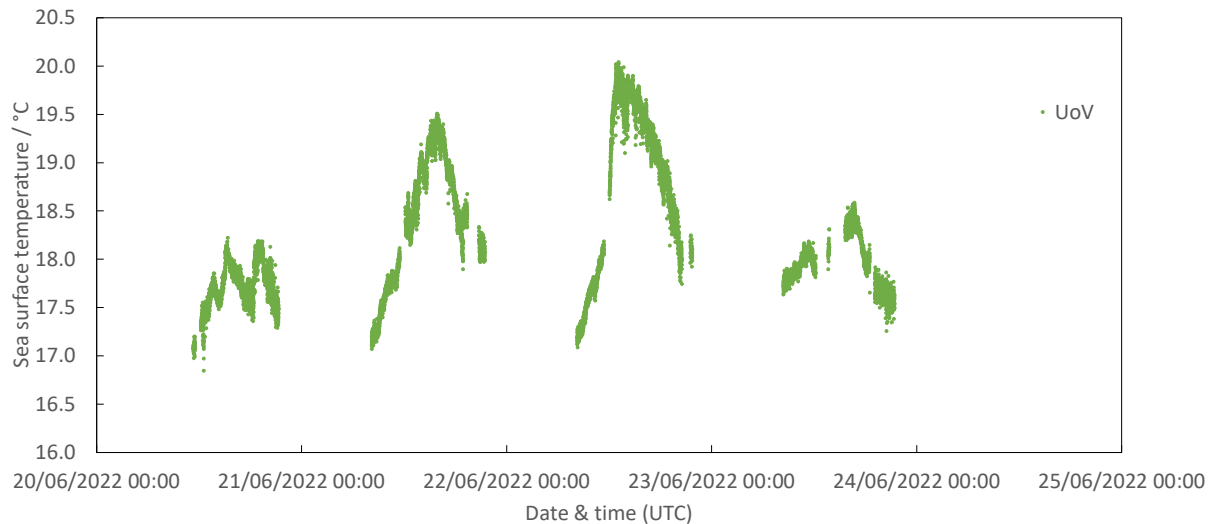
where $B_i(T)$ is averaged Planck's function for the channel i and a skin sea surface temperature T ; $\varepsilon_i(\theta, \phi)$ is the directional sea surface emissivity; and $L_i^{ref}(\theta, \phi)$ is the reflection of the downwelling sky radiance on the sea, where $L_{i\ atm}^{\downarrow}(\theta, \phi \pm \pi)$ is the incident sky radiance.

The CE312-2 Band 3 (10.2-11.0 μm) was selected for the measurements since this channel requires the lowest emissivity and atmospheric corrections [18]. A **viewing angle of 25°** was used to reduce the emissivity correction uncertainties but also the influence of the pier. The CE312-2 Unit 2 measured the water surface radiance at 25° (from Nadir) and the CE312-2 Unit 1 measured directly and simultaneously the downwelling sky radiance at 25° (from Zenith).

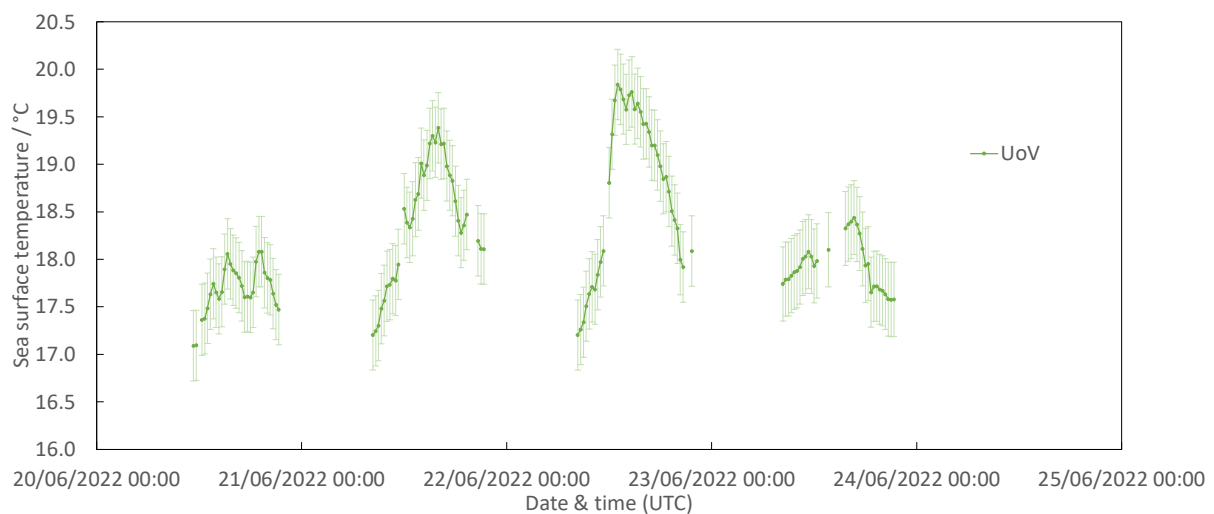
Radiometer usage (deployment), previous use of instrument and planned applications: The CE312 radiometers and methodologies have been used in many publications [11,16,17,18,20,21,22,23,24] and will be used for CAL/VAL activities and emissivity characterizations in the framework of different research projects.

5.1.2 Measured data

Figures 5 a), c) and d) show the measurement results reported by UoV. The SST a) is derived from the measured sea surface brightness temperature c) and sky brightness temperature d) assuming emissivity of 0.991. The SST averaged over 20 minutes is shown in b). Here, the error bar denotes the standard uncertainty of the measurement as described in Table 3, again averaged over 20 minutes.

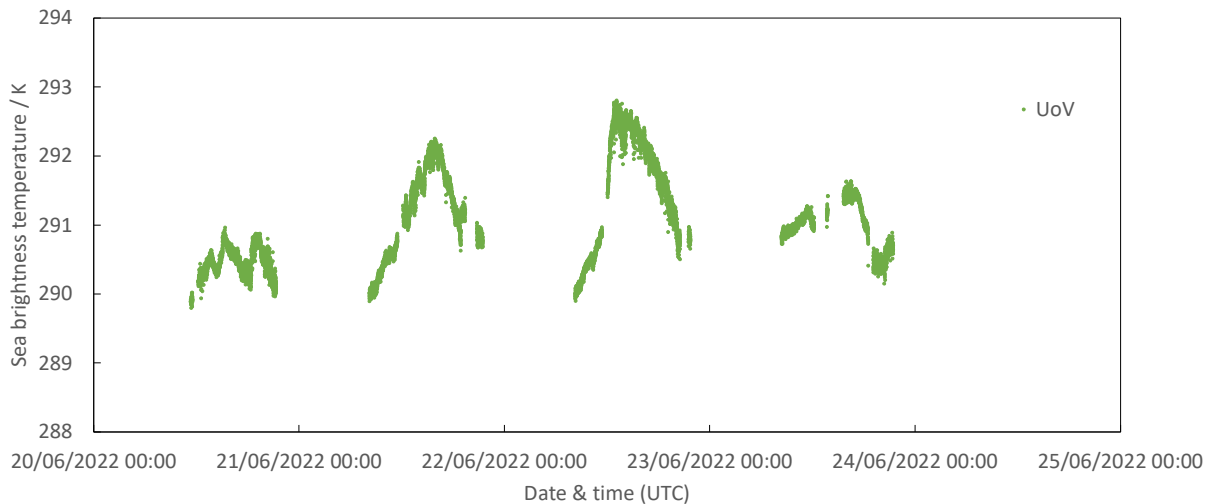


a) Sea surface temperature

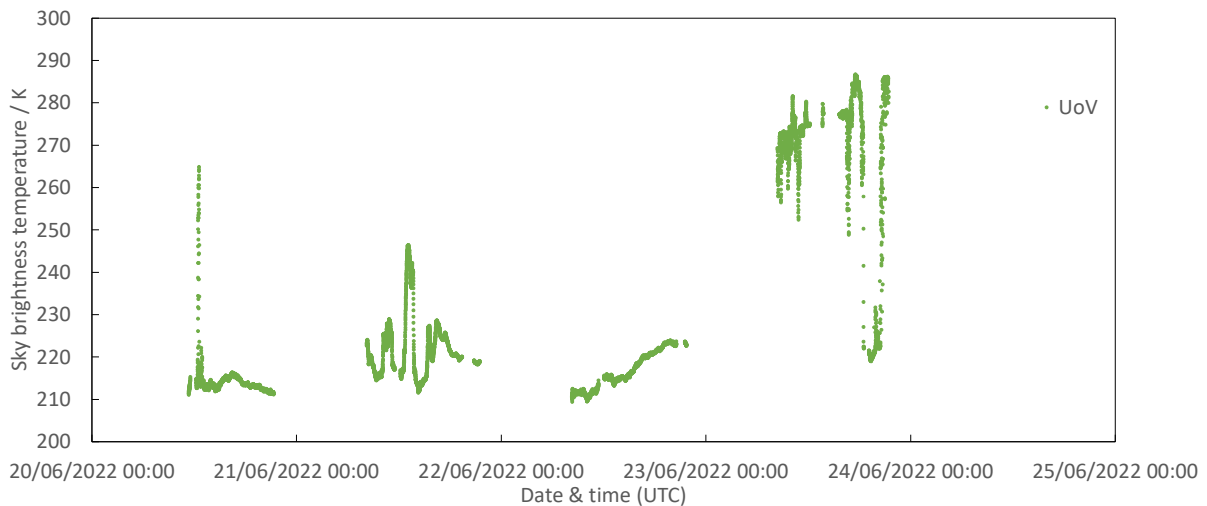


b) Sea surface temperature averaged over 20 minutes (Error bar denotes standard uncertainty)

Figure 5 Measurement by UoV (continued on next page)



c) Sea surface brightness temperature



d) Sky brightness temperature

Figure 5 Measurement by UoV (cont.)

5.2 MEASUREMENT BY KIT

5.2.1 Description of radiometers, route of traceability and uncertainty contributions

Make and type of Radiometers 'KIT-1' and 'KIT-2': Heitronics KT15.85 IIP

Outline Technical description of instrument: The KT15.85 IIP is a single channel radiometer based on a pyroelectric infrared detector. This type of sensor links radiance measurements via beam-chopping to internal reference temperature measurements and thermal drift can practically be eliminated. The KT15.85 IIP covers the spectral range from $9.6 \mu\text{m}$ to $11.5 \mu\text{m}$, has an uncertainty of about 0.3 K over the temperature range relevant to land surfaces and offers excellent long-term stability. The response time of the radiometer was set to 10 s . The type L6 lens used has a full-view angle of 8.3° . Radiometers KIT-1 ('surface') and KIT-2 ('sky') only differ in their calibrated temperature ranges, which are from -25°C to $+100^\circ\text{C}$ and -100°C to $+100^\circ\text{C}$, respectively.

Establishment or traceability route for primary calibration including date of last realisation and breakdown of uncertainty: Primary calibrations to within specifications were performed by Heitronics GmbH, Wiesbaden, Germany, on 2022-03-02 for KIT-1 (SN #9353; 'surface' radiometer) and on 2020-12-01 for KIT-2 (SN #13794; 'sky' radiometer) and verified using KIT's certified Landcal P80P BB. Breakdowns of uncertainties are provided in [AD-4]. The combined expanded uncertainty ($k = 2$) of the SST measurements made by the KIT during the current comparison was 440 mK.

Operational methodology during measurement campaign:

The two radiometers were mounted to a vertical 2 m long rod at the end of Boscombe pier. KIT-1 observed the sea surface at a view angle of 45° and KIT-2 pointed under the complementary angle into the sky. Given the view angle and KT15.85 IIP's central wavelength of 10.55 μm , the corresponding channel-effective emissivity was estimated as 0.986. Air temperature and humidity were also measured and all data were logged once per minute.

Radiometer usage (deployment), previous use of instrument and planned applications.

The primary usage of the Heitronics KT15.85 IIP radiometers is the in-situ determination of land surface temperature (LST) at one of KIT's permanent satellite LST validation sites. Before deploying the radiometers to a site, the radiometers are re-calibrated against KIT's Landcal P80P BB. Radiometer #9353 (KIT-1) was previously deployed at Gobabeb, Namibia, and then overhauled and re-calibrated by the manufacturer; radiometer #13794 (KIT-2) has only been used in the laboratory. Both radiometers will replace currently deployed instruments.

Table 4 Uncertainty Contributions associated with SST determination (KIT)

Instruments: Heitronics KT15.85 IIP

Temperature: 20 °C

Uncertainty Contribution	Type A Uncertainty in Value / (appropriate units)	Type B Uncertainty in Value / (appropriate units)	Standard uncertainty in Brightness temperature / °C
Repeatability of measurement	0.12 %		0.024
Reproducibility of measurement	0.12 %		0.024
Primary calibration		0.150 °C	0.150
Water emissivity		0.067 °C	0.067
Surface 'roughness'		0.033 °C	0.033
Angle of view to nadir		0.070 °C	0.070
Linearity of radiometer		0.053 °C	0.053
Drift since calibration		0.090 °C	0.090
Ambient temperature fluctuations		0.035 °C	0.035
		0.035 °C	0.035

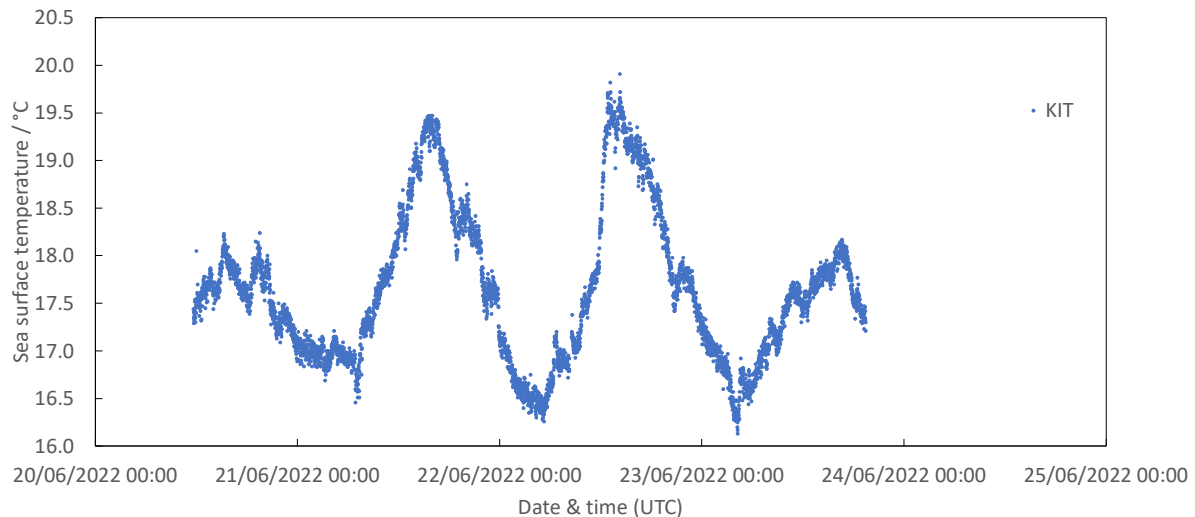
Atmospheric absorption/emission			
Combined uncertainty	0.17 %		0.218

Note: All uncertainty values are in standard uncertainties (i.e. $k = 1$)

Additional Type B uncertainty: 0.35 % of (target temp. – instrument temp.)

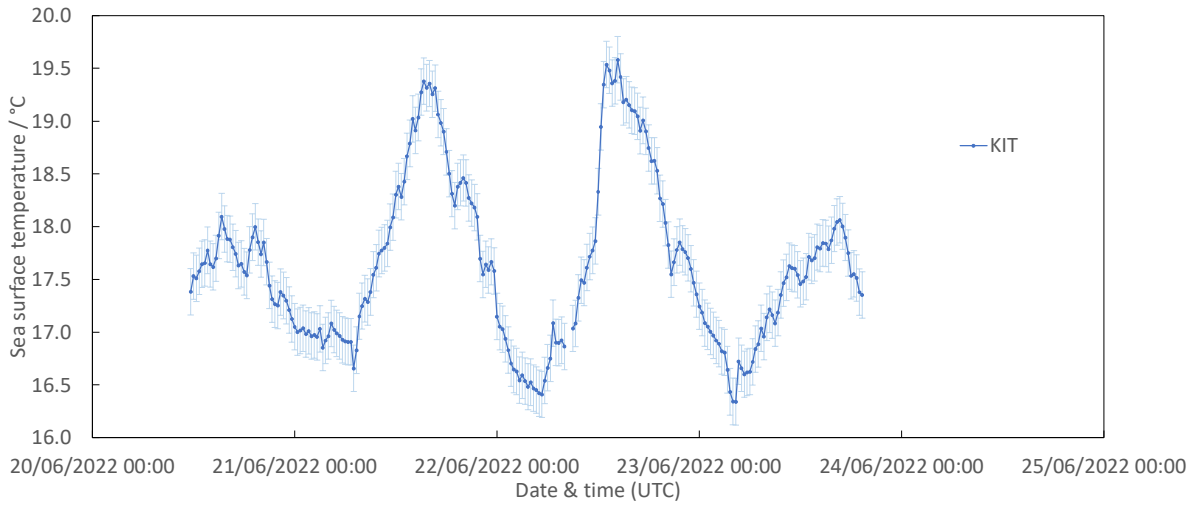
5.2.2 Measured data

Figures 6 a), c) and d) show the measurement results reported by KIT. The SST a) is derived from the measured sea surface brightness temperature c) and sky brightness temperature d) assuming emissivity of 0.986. The SST averaged over 20 minutes is shown in b). Here, the error bar denotes the standard uncertainty of the measurement as described in Table 4, again averaged over 20 minutes.

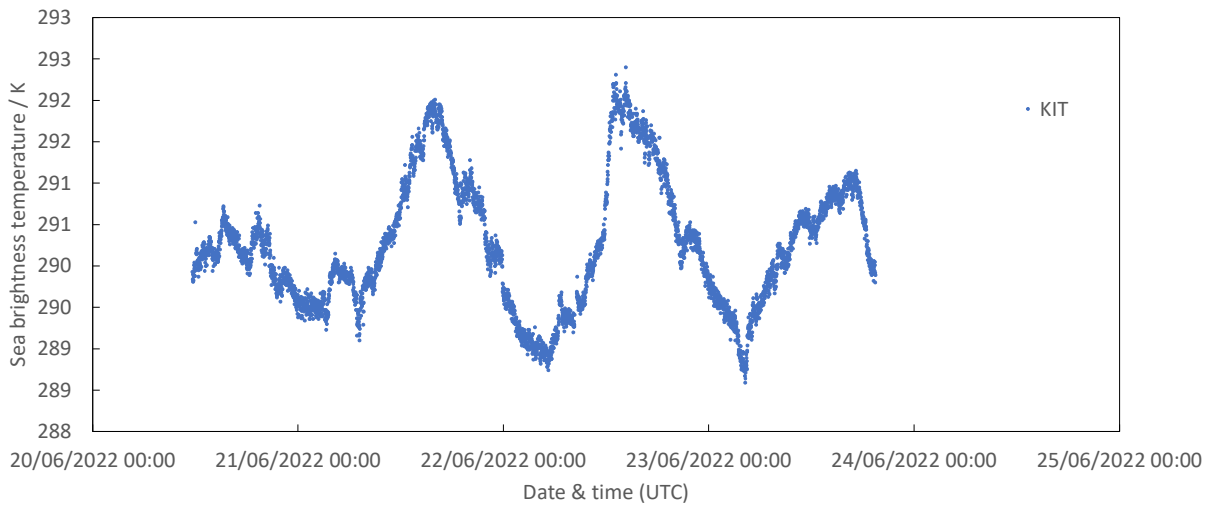


a) Sea surface temperature

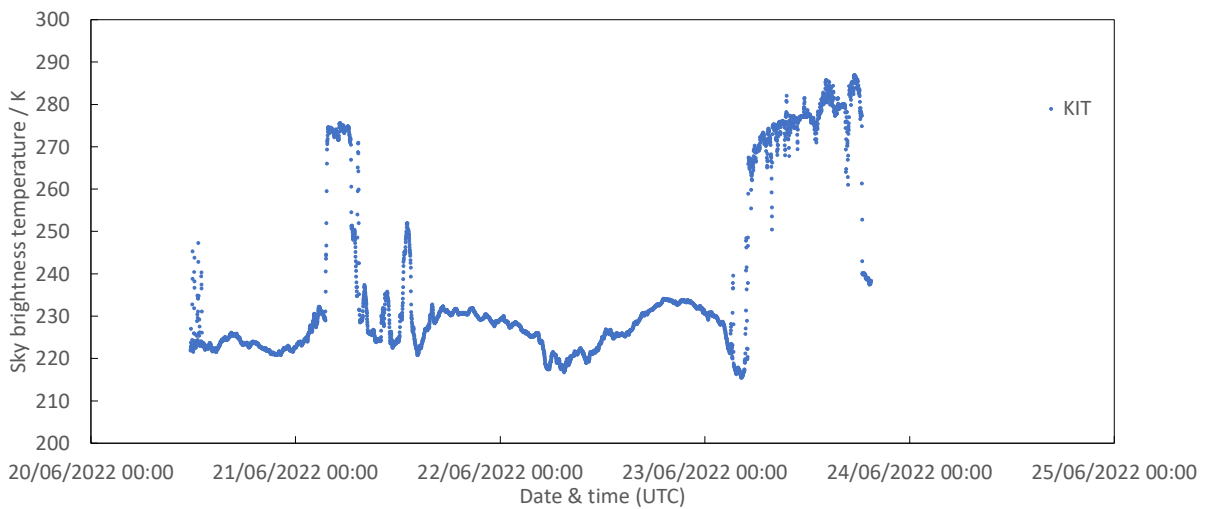
Figure 6 Measurement by KIT (continued on next page)



b) Sea surface temperature averaged over 20 minutes (Error bar denotes standard uncertainty)



c) Sea surface brightness temperature



d) Sky brightness temperature
Figure 6 Measurement by KIT

5.3 MEASUREMENT BY CSIRO

5.3.1 Description of radiometer, route of traceability and uncertainty contributions

Make and type of Radiometer: ISAR5-E

Outline Technical description of instrument:

Type: ISAR Field of view: 3.5 degree half angle Spectral band: 9.6-11.5 μm Temperature resolution : 0.01K

Full information on the ISAR radiometer can be found in [25,26].

Establishment or traceability route for primary calibration including date of last realisation and breakdown of uncertainty:

Last calibration: 19 June 2022 using CASOTS-II BB [27]

Post calibration: 24 June 2022 using CASOTS-II BB

Full model on ISAR uncertainty is details in [26].

The base line uncertainty of ISAR is 50 mK as that is the uncertainty of BB thermistors and therefore the ISAR cannot have a lower uncertainty than that. The combined expanded uncertainty ($k = 2$) of the SST measurements made by the CSIRO ISAR during the current comparison ranged from 80 mK to 660 mK with a mean of 130 mK.

Operational methodology during measurement campaign:

The ISAR was calibrated on 19 June 2022. It was installed on a wooden board which was extended over the edge of the pier and clamped using Delrin clamps secured to the board. The instrument was rotated so the two bottom dome nuts on the endcap without the connectors were both aligned. This is the exact orientation the instrument is calibrated on and ensures the calibration and deployment both occur with the instrument in the same orientation. The ISAR is autonomous and operated in a regular 4 measurement cycle, measuring the ambient BB, the heated BB, the sky view (25 degrees from nadir), and sea view, with 155 degrees from nadir being the sea view. An emissivity of 0.99164 was used for this campaign. The ISAR was calibrated on 24 June at the completion of this comparison and the data was processed using the data from both calibrations to adjust for degradation in the optical components.

Radiometer usage (deployment), previous use of instrument and planned applications.

This ISAR will be installed on Research Vessel (RV) Investigator, an Australian Science Vessel.

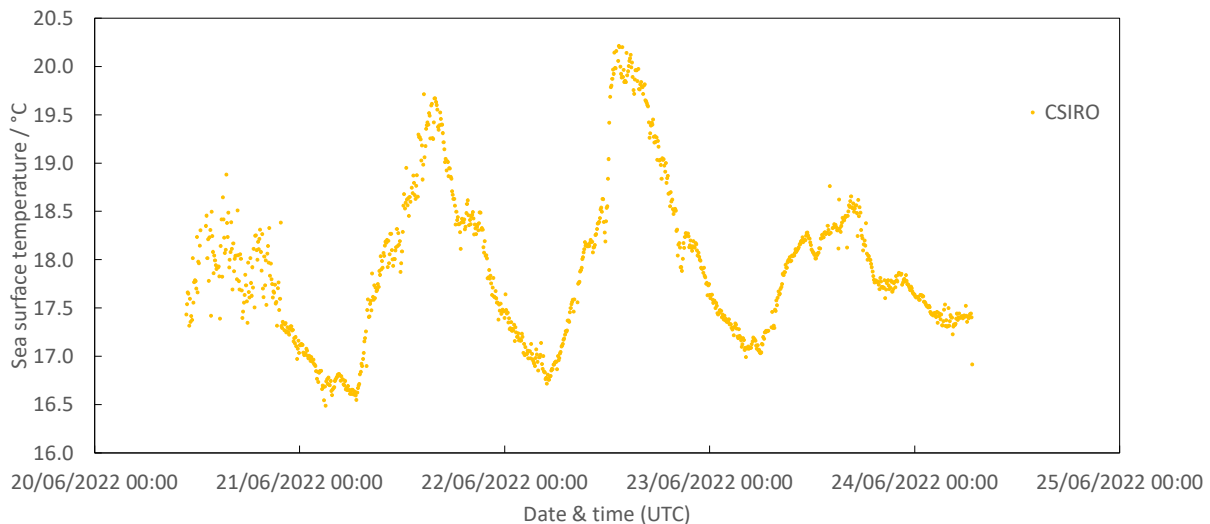
Table 5 Uncertainty Contributions associated with Radiometer (CSIRO)

e	Item	Uncertainty	Unit	Type
1	Detector linearity	<0.01 %	K month ⁻¹	B
2	Detector noise	~0.002	Volts	A
3	Detector accuracy	±0.5	K	B
4	ADC	±1(±76.3)	LSB (μV)	B
5	ADC accuracy	±0.1%	Range	B
6	ADC zero drift	±6	μV °C ⁻¹	B
7	Reference voltage 16-bit ADC	±15	mV	B
8	Reference voltage 12-bit ADC	±20	mV	B
9	Reference resistor	1	%	B
10	Reference resistor temperature coefficient	±100	Ppm °C ⁻¹	B
11	BB emissivity	±0.000178	Emissivity	B
12	Sea surface emissivity	±0.07	Emissivity	B
13	Steinhart–Hart approximation	±0.01	K	B
14	Radiate transfer approximation	±0.001	K	B
15	Thermistor	±0.05	K	B
16	Thermistor noise	~0.002	V	A

Note: All uncertainty values are in standard uncertainties (i.e. $k = 1$)

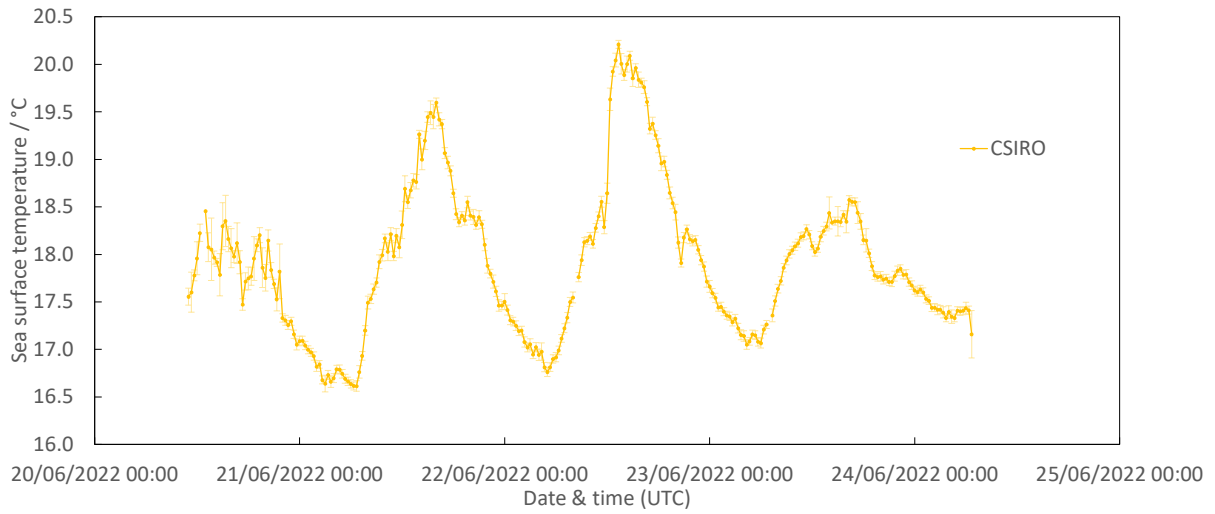
5.3.2 Measured data

Figures 7 a), c) and d) show the measurement results reported by CSIRO. The SST a) is derived from the measured sea surface brightness temperature c) and sky brightness temperature d) assuming emissivity of 0.9914-0.9920. The SST averaged over 20 minutes is shown in b). Here, the error bar denotes the standard uncertainty of the measurement as described in Table 5, again averaged over 20 minutes, although when the scatter is large, the type A component of this is replaced by the standard uncertainty of the measurement mean (i.e. the standard deviation divided by the square root of the number of averaged points).

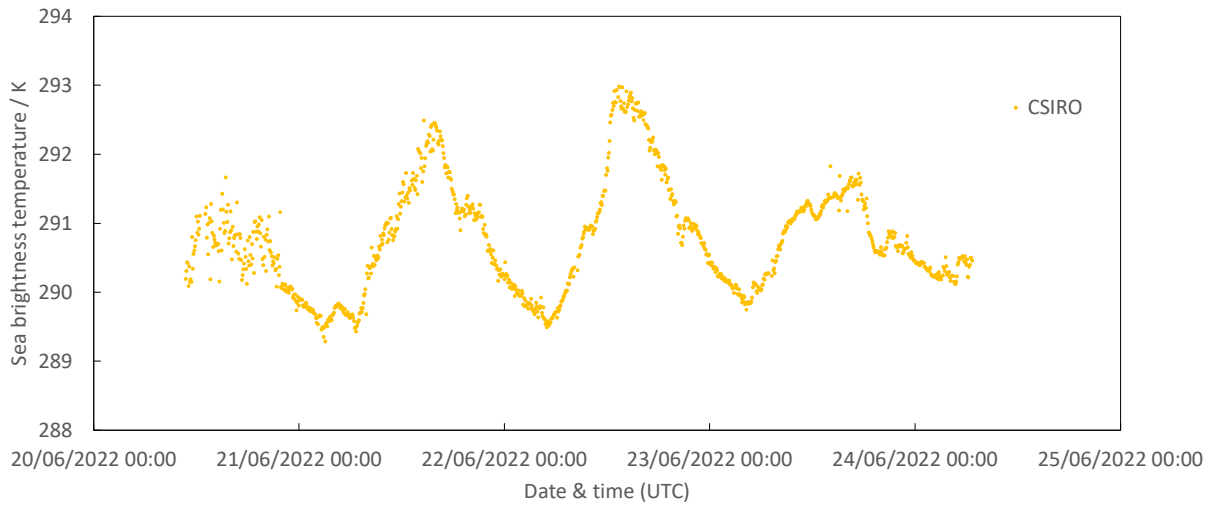


a) Sea surface temperature

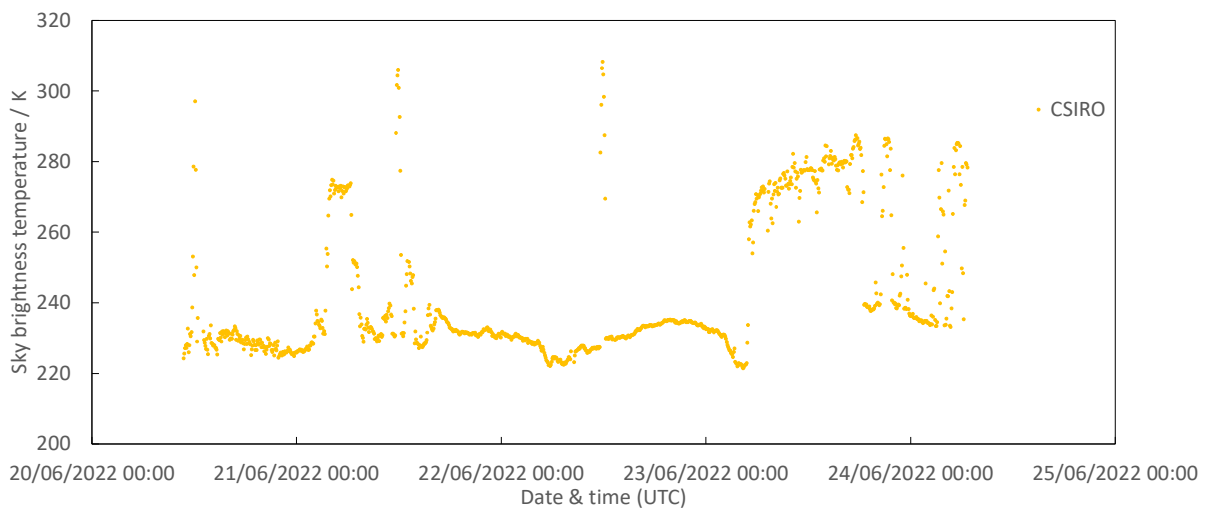
Figure 7 Measurement by CSIRO (continued on next page)



b) Sea surface temperature averaged over 20 minutes (Error bar denotes standard uncertainty)



c) Sea surface brightness temperature



d) Sky brightness temperature
Figure 7 Measurement by CSIRO (cont.)

5.4 MEASUREMENT BY RAL

5.4.1 Description of radiometer, route of traceability and uncertainty contributions

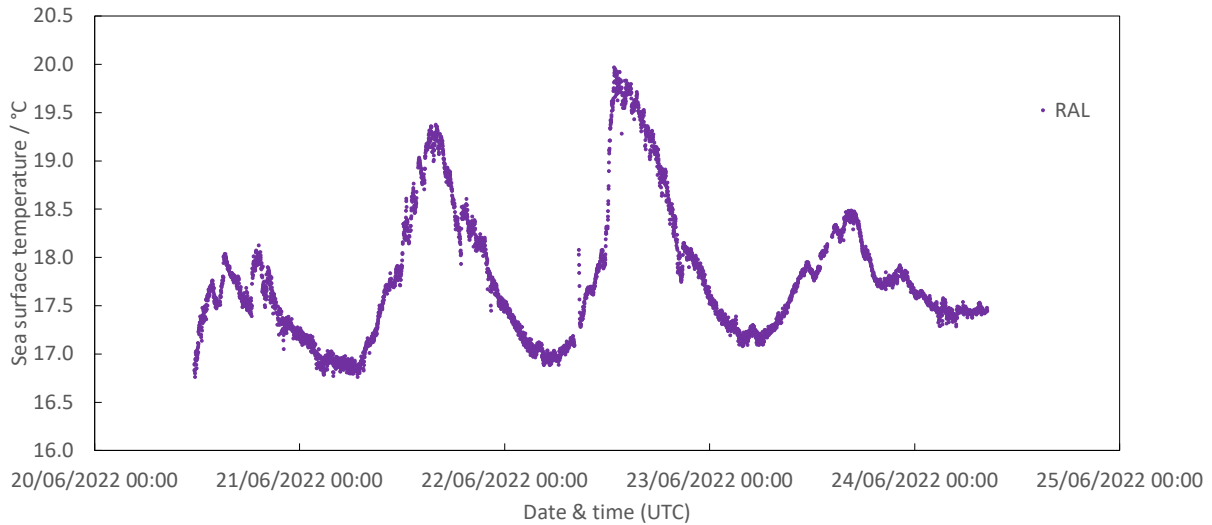
5.4.2 Description of radiometer, route of traceability and uncertainty contributions

The radiometer provided by the RAL was the Scanning Infrared Sea Surface Temperature Radiometer (SISTeR). SISTeR is a chopped, self-calibrating filter radiometer manufactured by RAL Space. It has a single-element DLaTGS pyroelectric detector, a filter wheel containing up to six band-defining filters and two internal reference BBs, one operating at ambient temperature and the other heated to approximately 17 K above ambient. During operation, the radiometer selected, with the aid of a scan mirror, successive views to each of the BBs and to the external scene in a repeated sequence. For SST measurements, the external measurements include views to the sea surface, and to the sky at the complementary angle. The instrument field of view is approximately 13° (full angle). During the comparison, a bandpass filter centred at 10.8 μm was used. The combined expanded uncertainty ($k = 2$) of the measurements made by the SISTeR radiometer during the comparison ranged from 30 mK to 220 mK with a mean of 90 mK. Further information on the SISTeR radiometer can be found in [28].

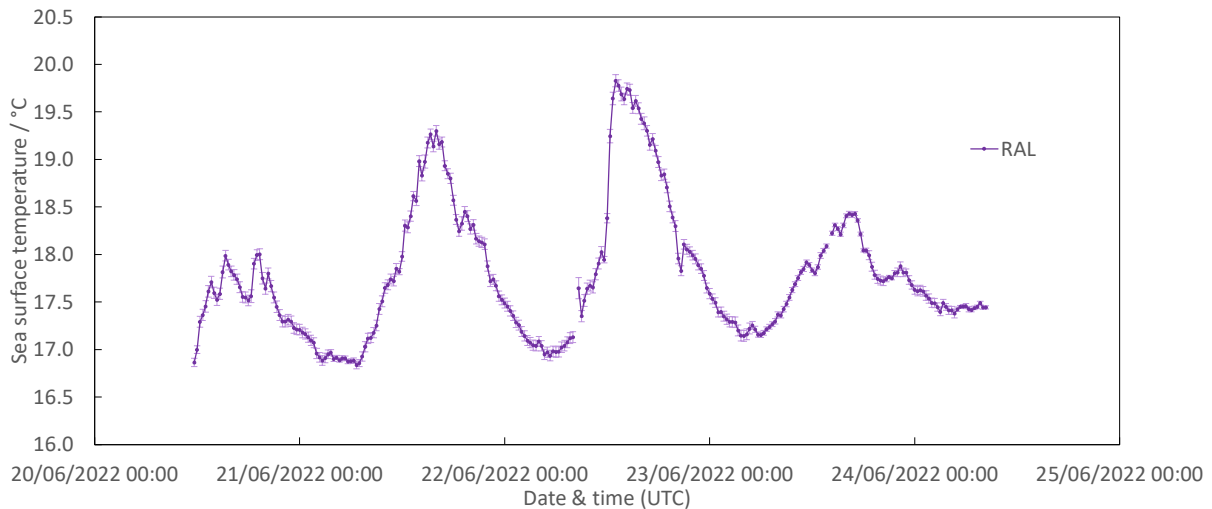
5.4.3 Measured data

RAL has reported a minor issue with the performance of the SISTeR radiometer during check measurements after the comparison, which cannot be rectified in time for the publication of this report. Therefore, the results presented here should be considered preliminary and may require correction later.

Figures 8 a) shows the measurement results reported by RAL. The SST a) is derived from the measured sea surface brightness temperature and sky brightness temperature with an assumed emissivity. The SST averaged over 20 minutes is shown in b). Here, the error bar denotes the standard uncertainty of the measurement as declared by the participant, again averaged over 20 minutes, although when the scatter is large, the type A component of this is replaced by the standard uncertainty of the measurement mean (i.e. the standard deviation divided by the square root of the number of averaged points).



a) Sea surface temperature



b) Sea surface temperature averaged over 20 minutes (Error bar denotes standard uncertainty)

Figure 8 Measurement by RAL

5.5 MEASUREMENT BY UoS

5.5.1 Description of radiometer, route of traceability and uncertainty contributions

Make and type of Radiometer: ISAR5-C serial number 3

Outline Technical description of instrument:

The ISAR is a self-calibration scanning radiometer, measuring at a single waveband between 9.6 to 11.5 μm . It uses two BBs for the calibration of the detector, one at ambient temperature and one at approximately 12 K above ambient temperature. The detector is a Heitronics KT15 with a field of view of 7 degrees. A detailed description of the ISAR radiometer can be found in [25,26].

Establishment or traceability route for primary calibration including date of last realisation and breakdown of uncertainty:

The traceability route for ISAR is through the internal BB thermistors which are traceable to NIST. The internal calibration is verified with an external water BB (CASOTS-II, see [27]) before and after each deployment. Both ISAR and CASOTS get verified by NPL every five to six years at the radiometer inter-comparisons to ensure their performance and uncertainty.

The ISAR uncertainty model is described in [26] and propagates the uncertainties of each component through the measurement equation. This produces a per measurement uncertainty, which is split into Type A and Type B uncertainties as well as an instrument and a measurement uncertainty. Figure 9 shows a flow chart of the uncertainty components propagated through the measurement equation and table 6 shows the associated uncertainties of the main components. The base line uncertainty of ISAR is 50 mK as that is the uncertainty of BB thermistors and therefore the ISAR cannot have a lower uncertainty than that. The combined expanded uncertainty ($k = 2$) of the SST measurements made by the UoS ISAR during the current comparison ranged from 80 mK to 350 mK with a mean of 110 mK.

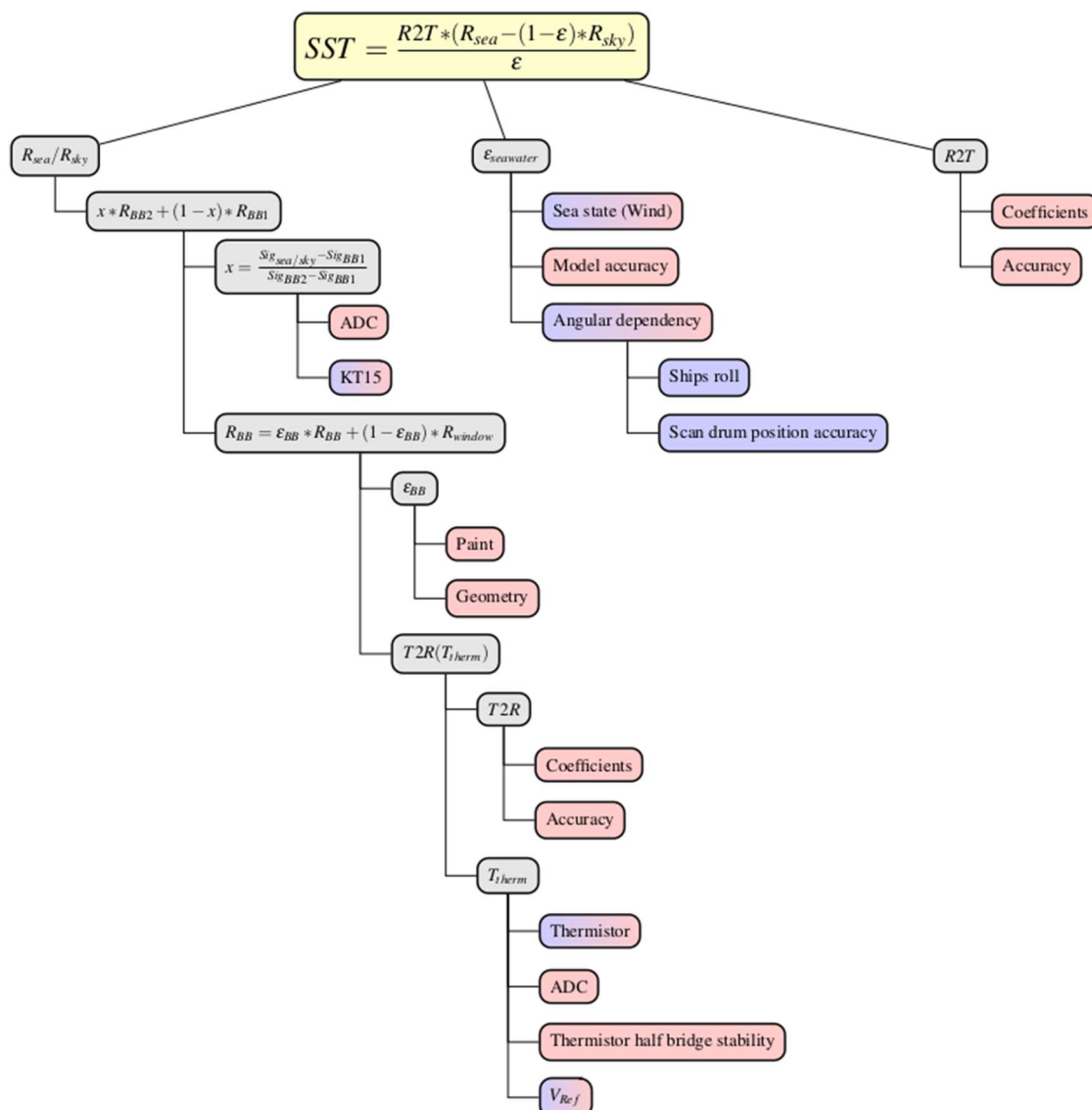


Figure 9: ISAR uncertainty model, from [26]

Table 6 Uncertainty Contributions associated with Radiometer (UoS).

e	Item	Uncertainty	Unit	Type
1	Detector linearity	<0.01 %	K month ⁻¹	B
2	Detector noise	~0.002	Volts	A
3	Detector accuracy	±0.5	K	B
4	ADC	±1(±76.3)	LSB (μV)	B
5	ADC accuracy	±0.1%	Range	B
6	ADC zero drift	±6	μV °C ⁻¹	B
7	Reference voltage 16-bit ADC	±15	mV	B
8	Reference voltage 12-bit ADC	±20	mV	B
9	Reference resistor	1	%	B
10	Reference resistor temperature coefficient	±100	Ppm °C ⁻¹	B
11	BB emissivity	±0.000178	Emissivity	B
12	Sea surface emissivity	±0.07	Emissivity	B
13	Steinhart–Hart approximation	±0.01	K	B
14	Radiate transfer approximation	±0.001	K	B
15	Thermistor	±0.05	K	B
16	Thermistor noise	~0.002	V	A

Note: All uncertainty values are in standard uncertainties (i.e. $k = 1$)

Operational methodology during measurement campaign:

The ISAR was installed on a wooden board which was extended over the edge of the pier in such a way that the fall arrest wires were cleared. The wooden board was mounted to the pier with u-clamps. The instrument alignment was verified by reading the onboard roll and pitch sensor. The ISAR was configured to a six measurements cycle, ambient BB, heated BB, three sky views at 165, 155, 145 degrees from nadir, and one sea view at 25 degrees from nadir. Nadir is assumed to be looking straight down from the instrument axis. Some data on the morning of the first day (20.06.2022) was not used as the configuration of the instrument was wrong (it was still ruining the laboratory measurement cycle from the week before) and this was not discovered until after lunch.

The ISAR was calibrated against the UoS CASOTS-II before the laboratory comparison measurements at NPL and was calibrated again after the Boscombe pier deployment to ensure it was operating correctly during the measurements.

Radiometer usage (deployment), previous use of instrument and planned applications.

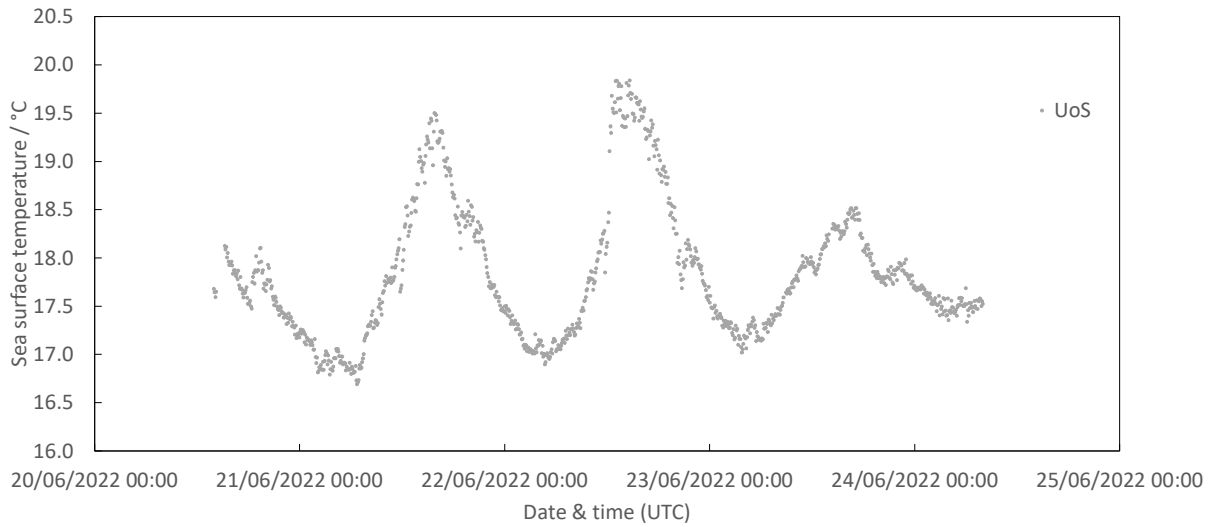
The UoS ISARs (S/N 2,3 and 12) are mainly used on ferries traveling between the UK and Spain, but are also used on mainly UK research vessels and on opportunistic measurement campaigns on ICE (Greenland 2011 and 2016 or land Namibia 2017).

The UoS ISAR data is processed to the International SST FRM Radiometer Network (ISFRN) Level 2 in situ radiometric data product (L2R) netcdf data format and stored at the ships4sst archive at National Institute for Ocean Science (IFREMER). These data are used by European Organisation for the Exploitation of Meteorological Satellites (EUMETSAT) to produce the validation match-up database for the Sea and Land Surface Temperature Radiometer (SLSTR) sensor on the ESA Sentinel 3 satellite.

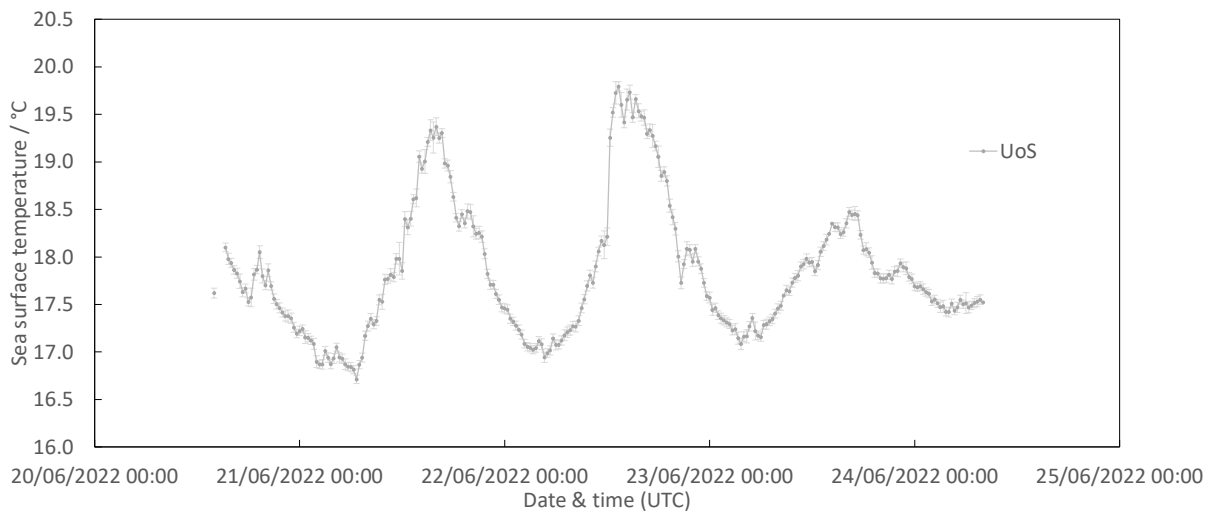
5.5.2 Measured data

Figures 10 a), c) and d) show the measurement results reported by UoS. The SST a) is derived from the measured sea surface brightness temperature c) and sky brightness temperature d) assuming emissivity of 0.991635. The SST averaged over 20 minutes is shown in b). Here, the error bar denotes the standard uncertainty of the measurement as described in Table 6, again averaged over 20 minutes, although when the scatter is large, the type A component of

this is replaced by the standard uncertainty of the measurement mean (i.e. the standard deviation divided by the square root of the number of averaged points).

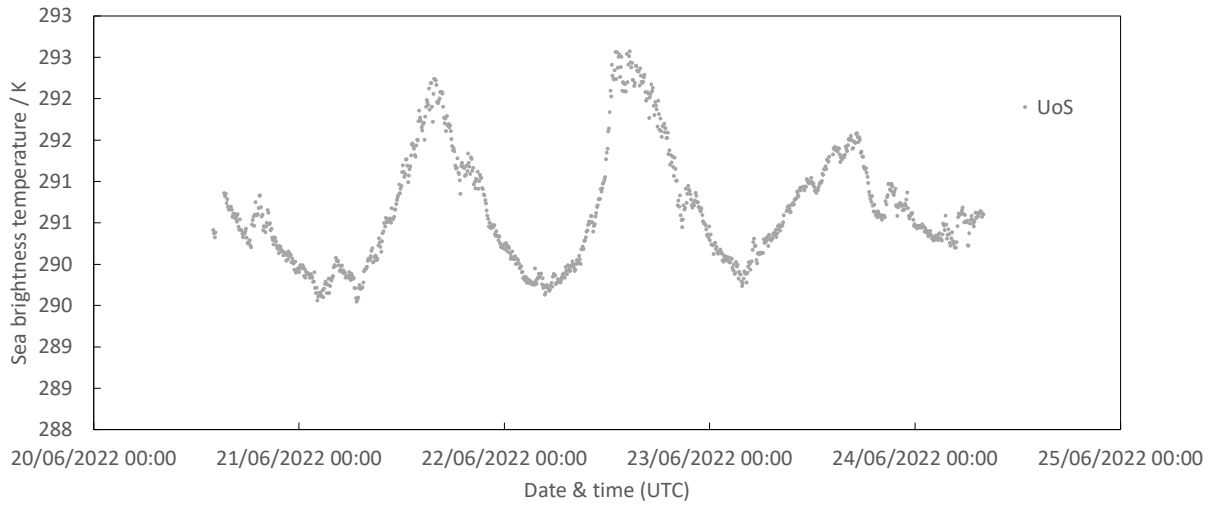


a) Sea surface temperature

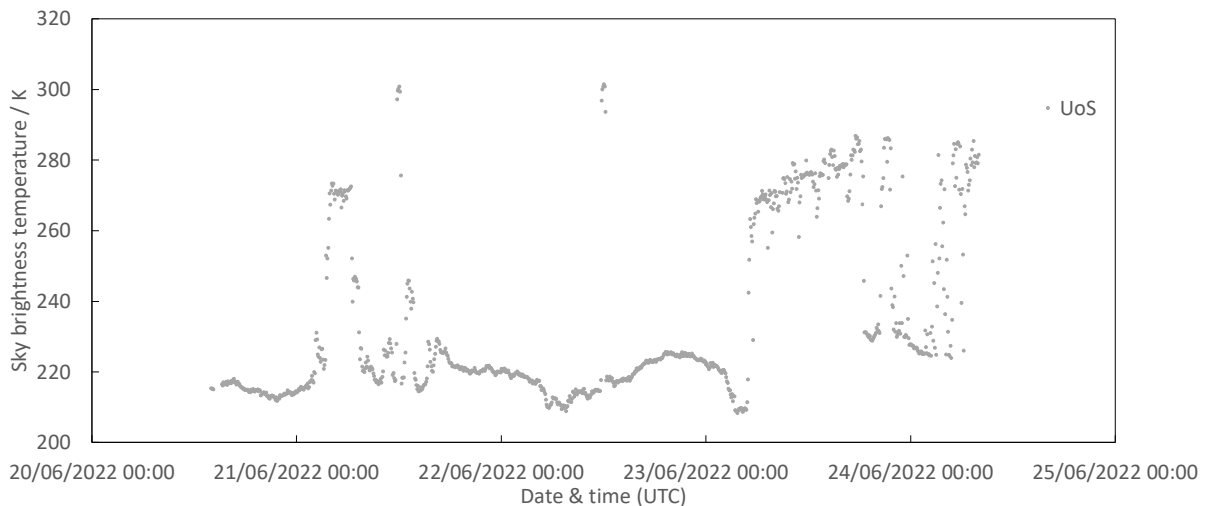


b) Sea surface temperature averaged over 20 minutes (Error bar denotes standard uncertainty)

Figure 10 Measurement by UoS (continued on next page)



c) Sea surface brightness temperature



d) Sky brightness temperature

Figure 10 Measurement by UoS (cont.)

5.6 MEASUREMENT BY DMI

5.6.1 Description of radiometer, route of traceability and uncertainty contributions

Make and type of Radiometer: ISAR5-D

Outline Technical description of instrument:

The ISAR is a self-calibration scanning radiometer, measuring at a single waveband between 9.6 to 11.5 μm . It uses two BBs for the calibration of the detector, one at ambient temperature and one at approximately 12 K above ambient temperature. The detector is a Heitronics KT15 with a field of view of 7 degrees. A detailed description of the ISAR radiometer can be found in [25,26].

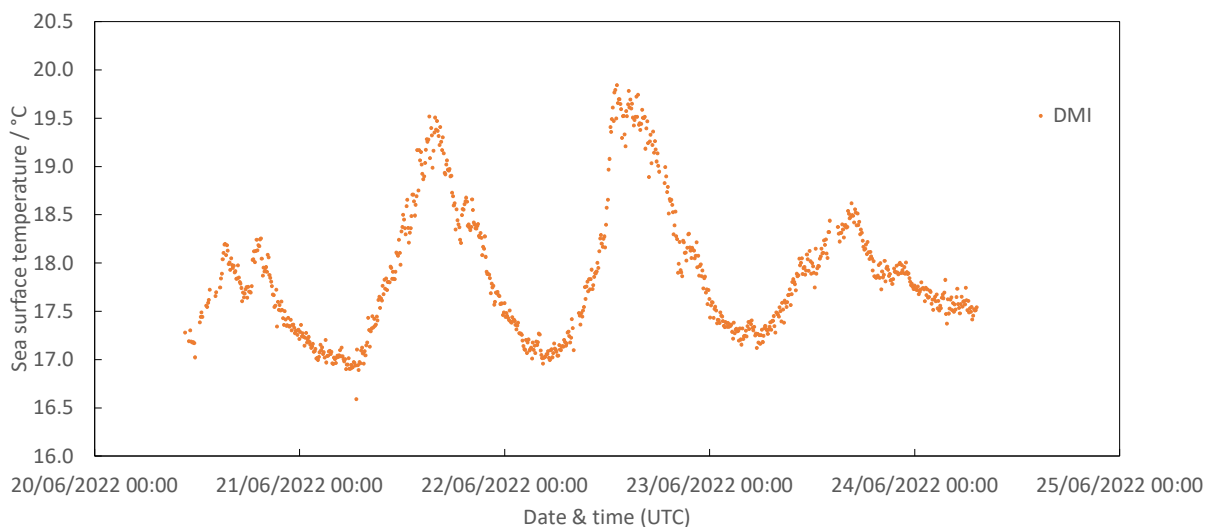
Establishment or traceability route for primary calibration including date of last realisation and breakdown of uncertainty:

The traceability route for ISAR is through the internal BB thermistors which are traceable to NIST. This radiometer was calibrated with the aid of a CASOTS-II BB [27].

The ISAR uncertainty model is described in [26] and propagates the uncertainties of each component through the measurement equation. This produces a per measurement uncertainty, which is split into Type A and Type B uncertainties as well as an instrument and a measurement uncertainty. The base line uncertainty of ISAR is 50 mK as that is the uncertainty of BB thermistors and therefore the ISAR cannot have a lower uncertainty than that. The combined expanded uncertainty ($k = 2$) of the SST measurements made by the DMI ISAR during the current comparison ranged from 90 mK to 480 mK with a mean of 130 mK.

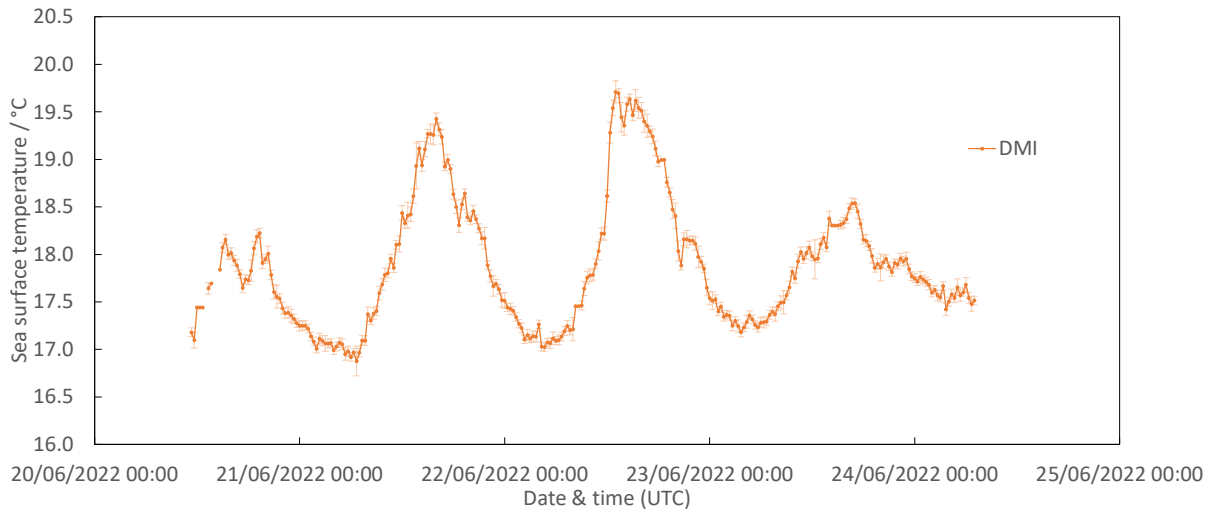
5.6.2 Measured data

Figures 11 a), c) and d) show the measurement results reported by DMI. The SST a) is derived from the measured sea surface brightness temperature c) and sky brightness temperature d) assuming emissivity of 0.9914-0.9918. The SST averaged over 20 minutes is shown in b). Here, the error bar denotes the standard uncertainty of the measurement as declared by the participant, again averaged over 20 minutes, although when the scatter is large, the type A component of this is replaced by the standard uncertainty of the measurement mean (i.e. the standard deviation divided by the square root of the number of averaged points).

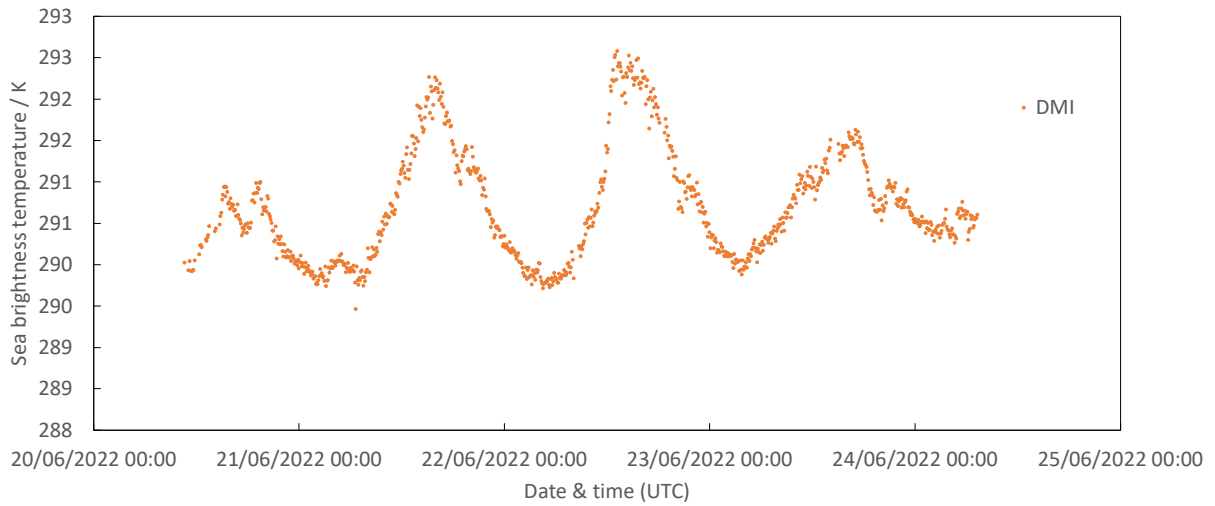


a) Sea surface temperature

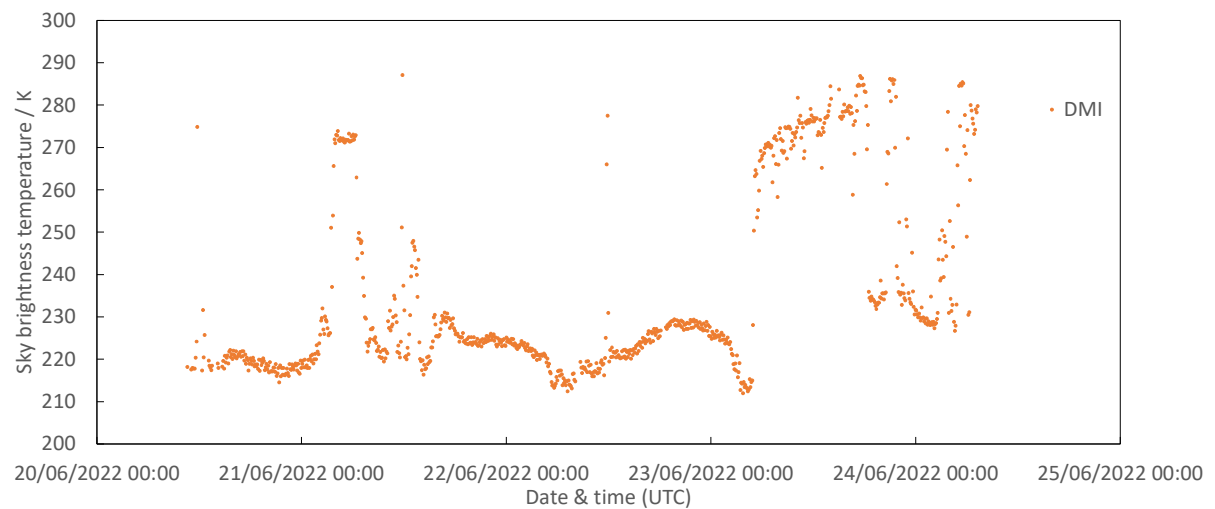
Figure 11 Measurement by DMI (continued on next page)



b) Sea surface temperature averaged over 20 minutes (Error bar denotes standard uncertainty)



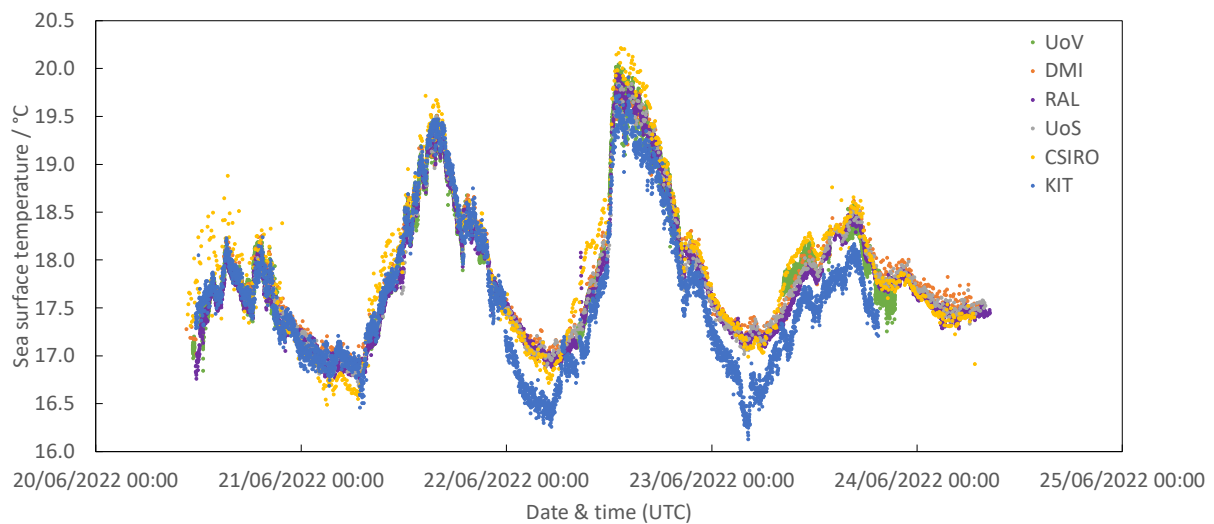
c) Sea surface brightness temperature



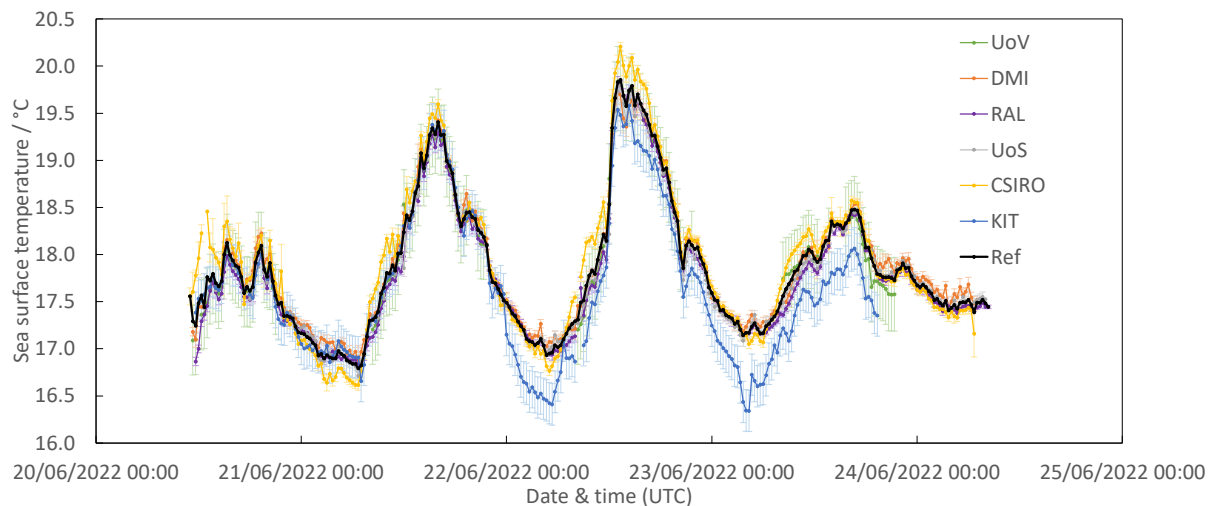
d) Sky brightness temperature
Figure 11 Measurement by DMI (cont.)

6 COMPARISON RESULT

Figure 12 a), d) and e) show the measurement results reported by all participants. The SST a) and b), sea d) and sky e) brightness temperatures are those shown individually in Figs. 5 to 8 and 10 to 11, overlaid. The simple mean of the SST averaged over 20 minutes b) is used to calculate the reference value. Since UoV did not make measurements during the night, UoV data are reflected only in the comparison reference value during daytime hours. KIT measurement shows an abrupt shift of approximately $-0.4\text{ }^{\circ}\text{C}$ just before midnight of 21 June 2022, so KIT data on or after 22 June 2022 were also excluded from evaluating the reference value. Although RAL reports a drift in the SISTeR internal BB and therefore claims the results may require adjustment, RAL data have been included in the evaluation of the reference value since the effect of the reported 20 mK drift is insignificantly small compared to the scatter among participants. The reference value ('Ref') is shown in b). The difference from the reference value was then evaluated for each participant and the result is plotted in Fig. 12 c), with the error bar denoting the standard uncertainty.

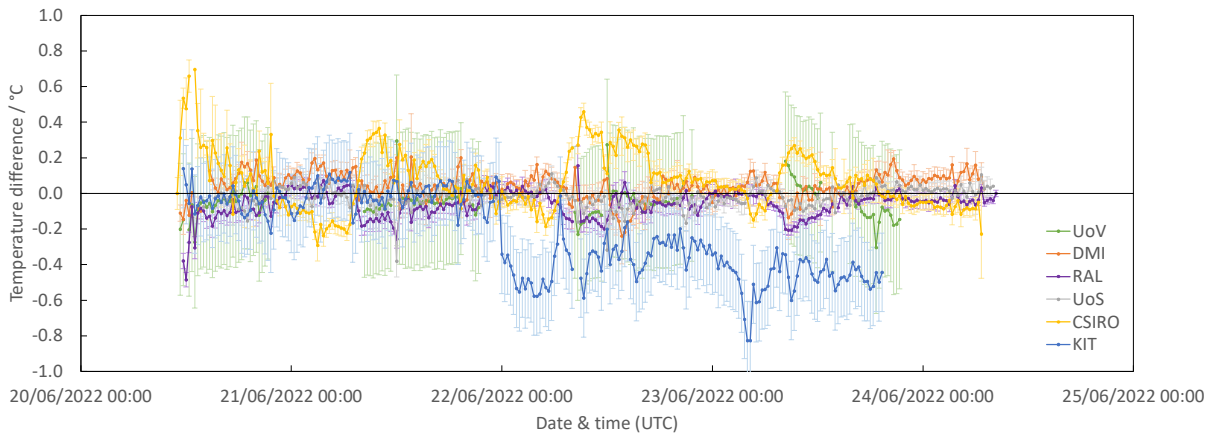


a) Sea surface temperature

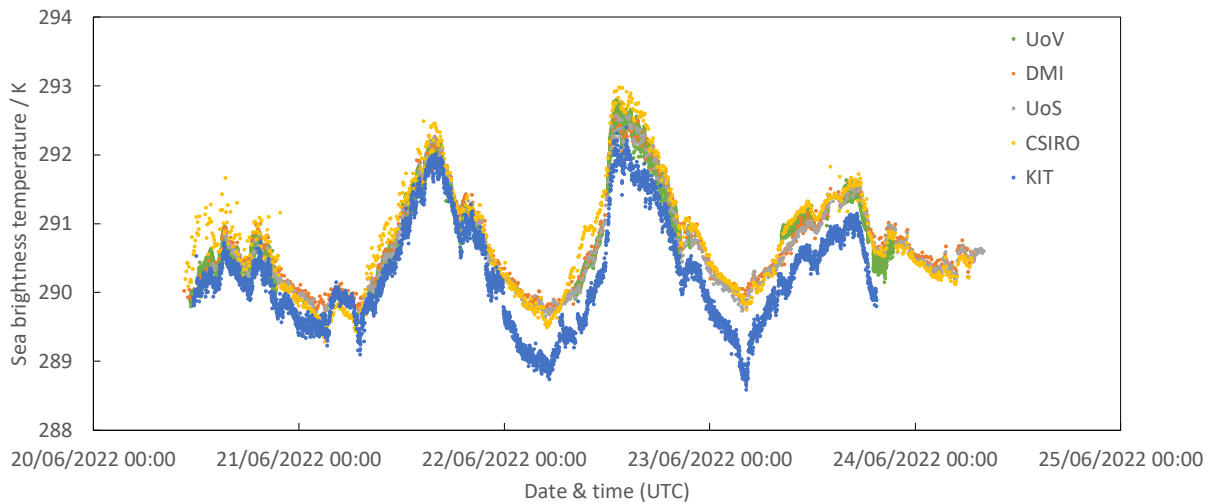


b) Sea surface temperature averaged over 20 minutes. (Error bar denotes standard uncertainty.) Reference value taken as the arithmetic mean of all participants, excluding KIT on or after 22 June 2022, is also plotted.

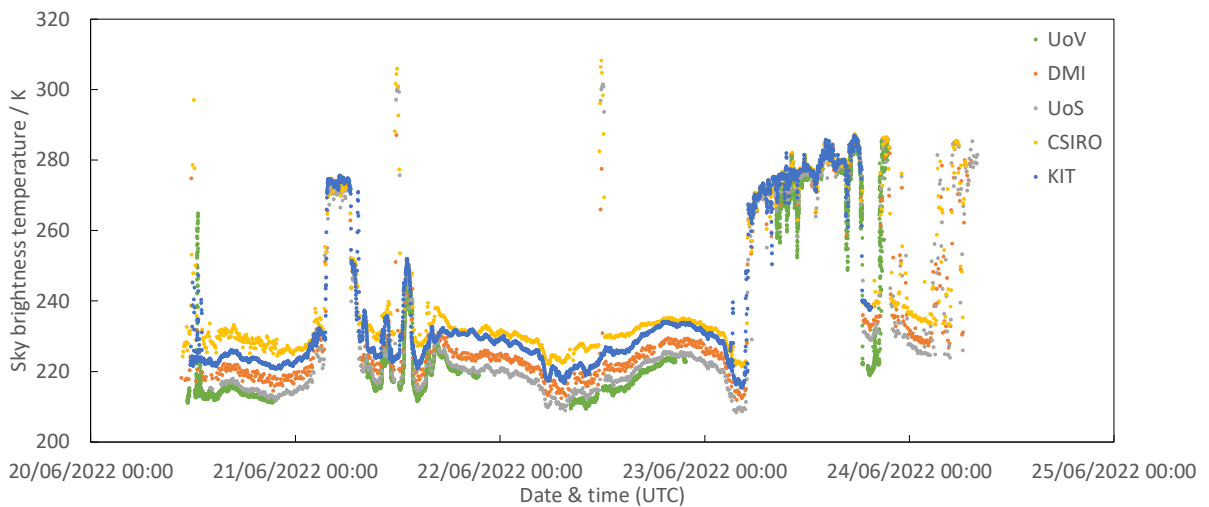
Figure 12 Comparison results (continued on next page)



c) Difference of sea surface temperature averaged over 20 minutes from reference value. (Error bar denotes standard uncertainty.) Reference value is the arithmetic mean of all participants excluding KIT on or after 22 June 2022.



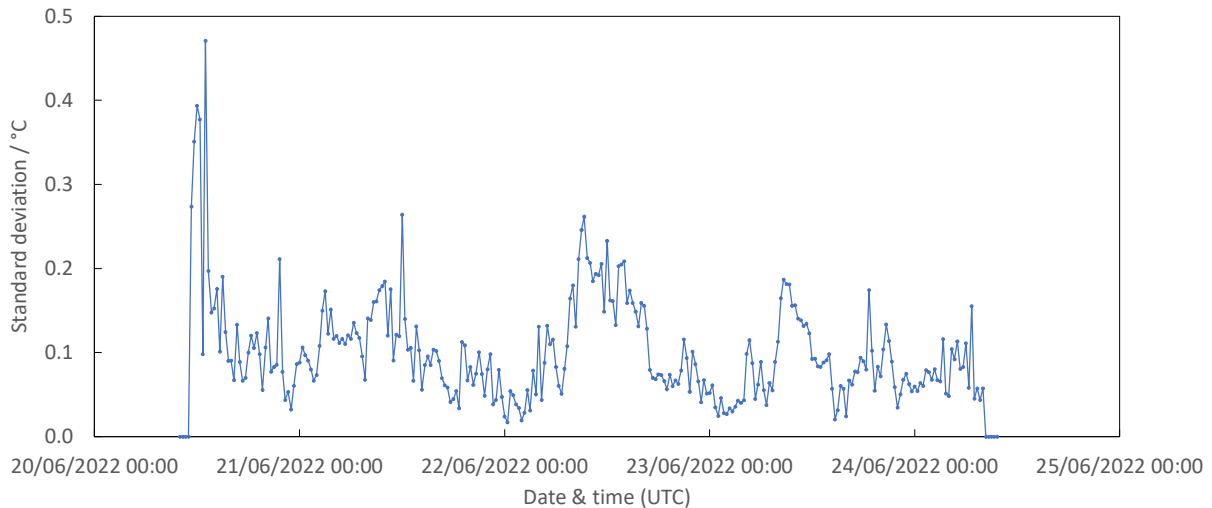
d) Sea surface brightness temperature (RAL data not reported)



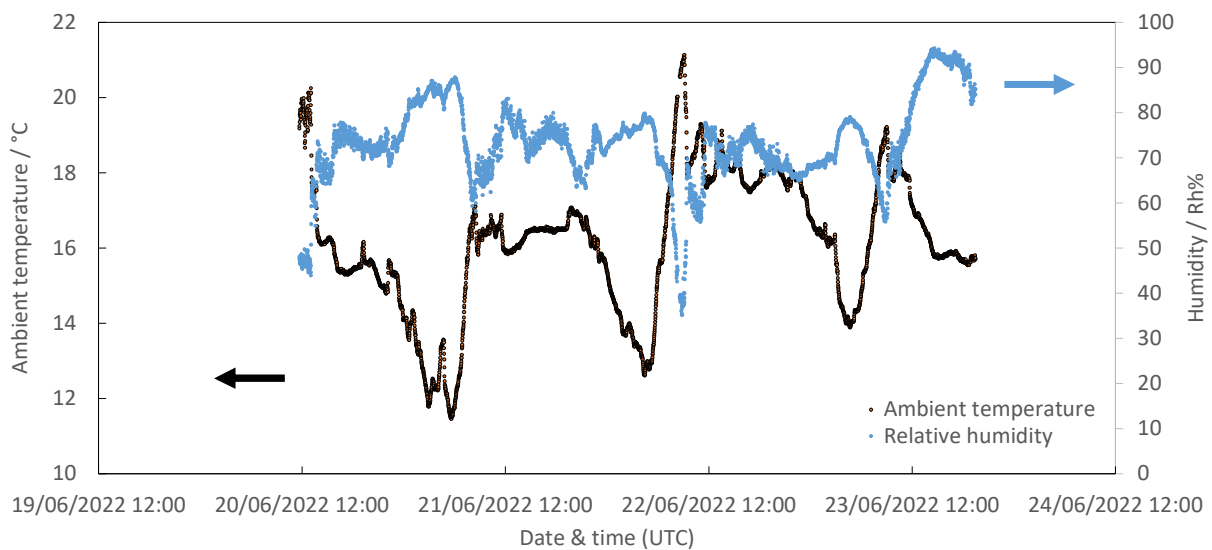
e) Sky brightness temperature (RAL data not reported)

Figure 12 Comparison results (cont.)

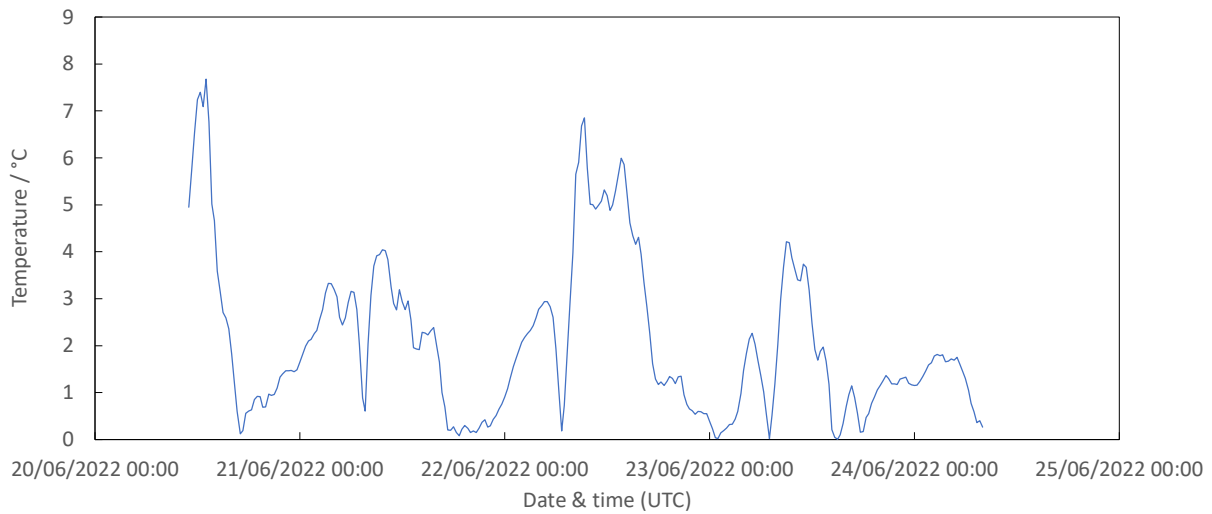
Fig. 13, a) shows the scatter of the participants' measured SST over time evaluated as the standard deviation for each twenty-minute average. KIT data on or after 22 June 2022 were not included for the same reason as for the evaluation of the reference value. Possible influencing factors, such as ambient temperature and humidity b) and absolute difference between the average internal BB temperature for the three ISARs and the ambient temperature c) were considered and are plotted.



a) Standard deviation of the SST measured by participants excluding KIT after 22 June 2022.

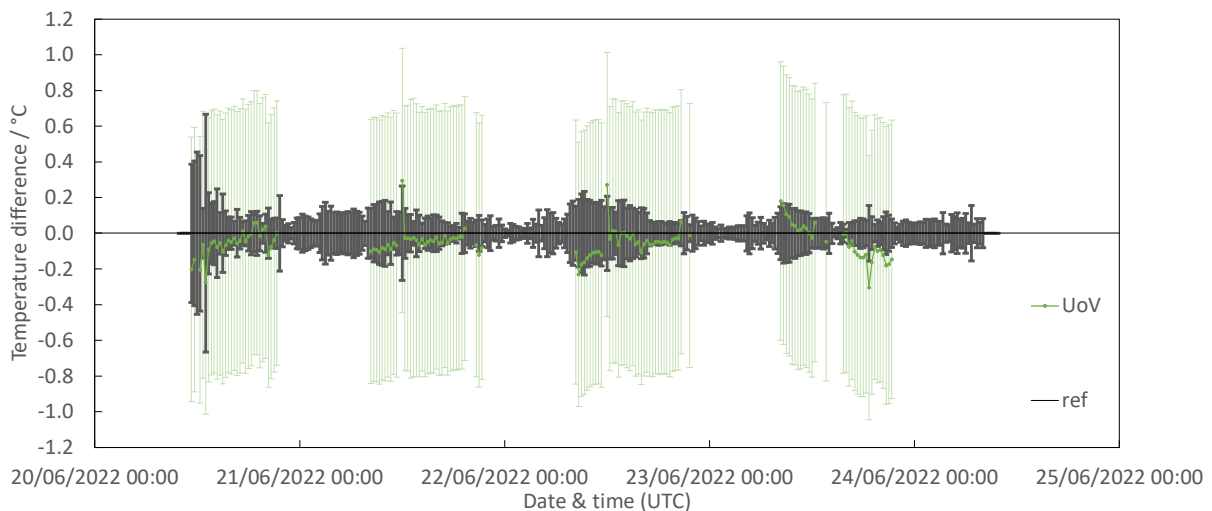


b) Ambient temperature and relative humidity (measurement provided by KIT)
 Figure 13 Scatter of measurement and influencing factors (continued on next page)

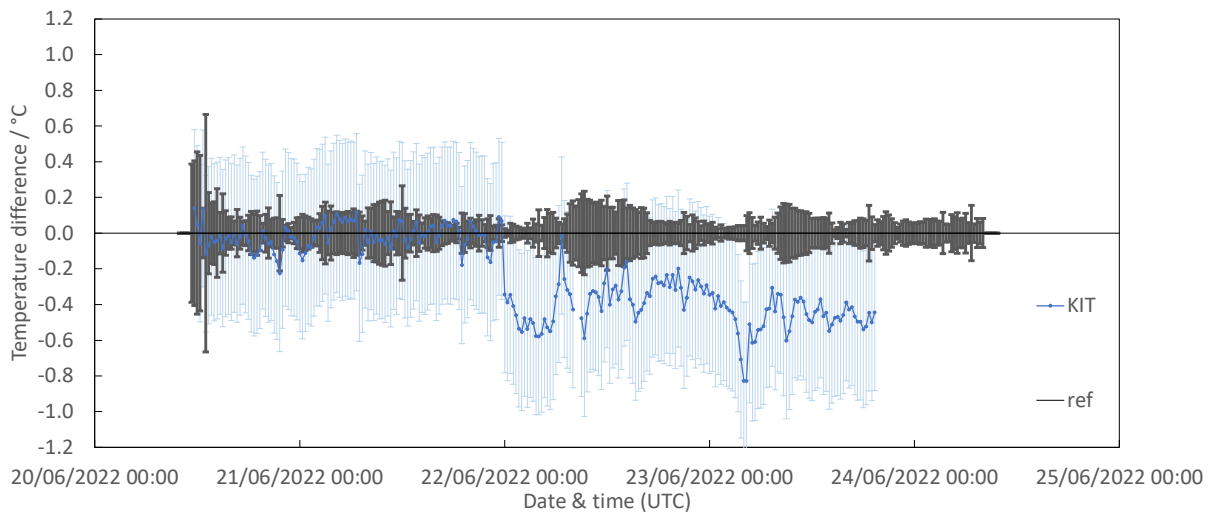


c) Absolute difference between ISAR internal BB temperature and ambient temperature
 Figure 13 Scatter of measurement and influencing factors (cont.)

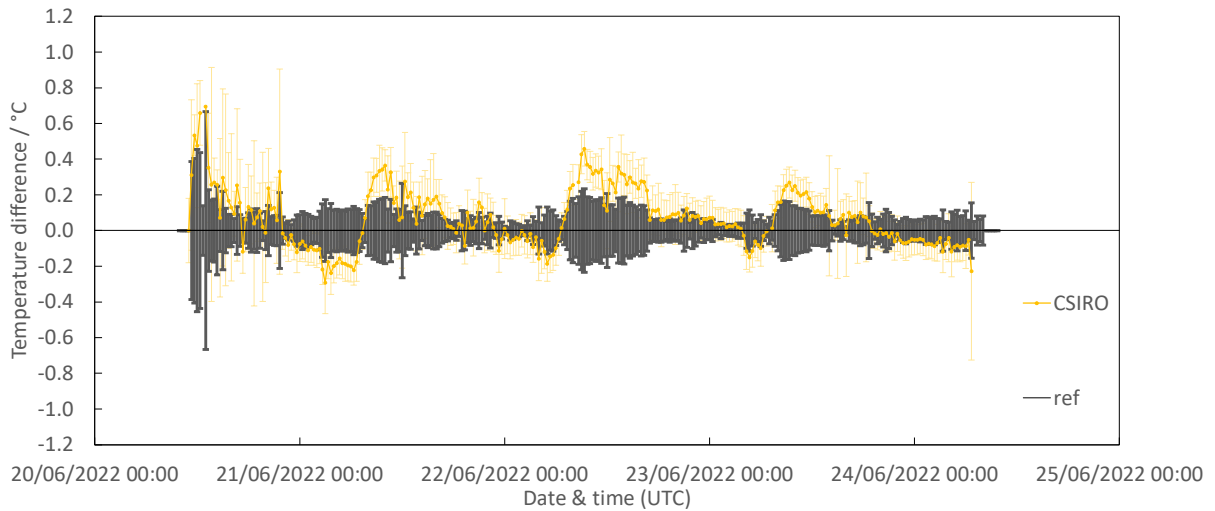
The agreements of each participant's data with the reference value were evaluated and are shown in Figs. 14 a) to 14 f). The vertical axis is the difference of the participant value from the reference value. The reference value is evaluated as the simple mean of the participants' values (after taking the average over each 20 minutes' interval) excluding KIT on or after 22 June 2022. The uncertainty of the reference value is the standard deviation of the participants' values. The plots show two error bars: the one for the temperature difference is the uncertainty of the participant measurement, the other black bar around zero ('ref') is the uncertainty of the reference value. Both are evaluated for the expanded uncertainty for $k=2$. Note that RAL detected a minor instability in the internal BB and the results in Fig. 14 d) are not final.



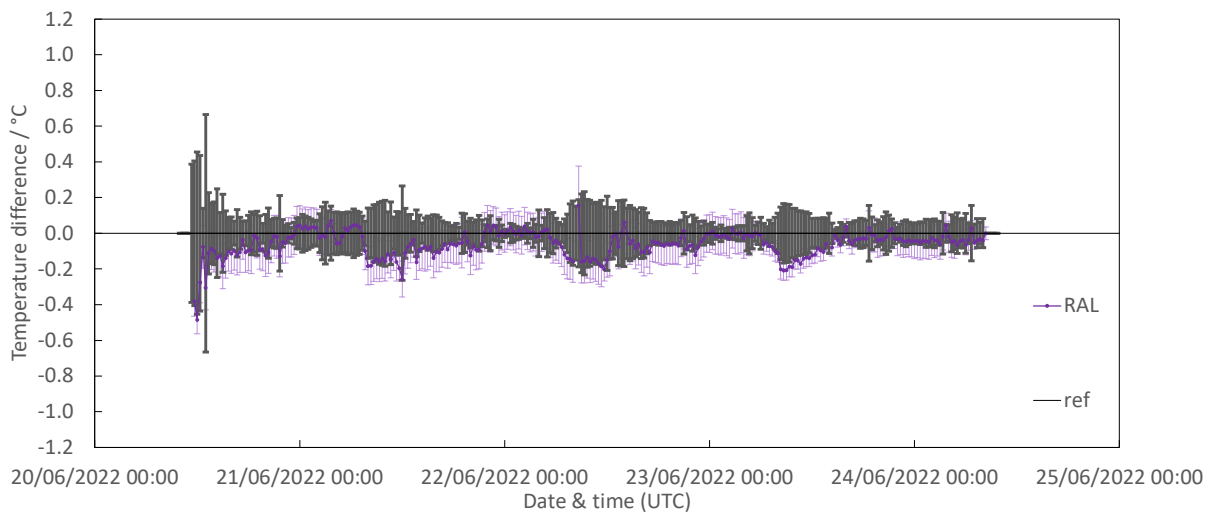
a) UoV (mean difference: $-0.049\text{ }^{\circ}\text{C}$, standard deviation of difference: $0.082\text{ }^{\circ}\text{C}$)
 Figure 14 Agreement with reference value (continued on next page)



b) KIT (mean diff.: $-0.017\text{ }^{\circ}\text{C}$, up to 21 June 2022, $-0.414\text{ }^{\circ}\text{C}$ on or after 22 June 2022, standard deviation of diff.: $0.073\text{ }^{\circ}\text{C}$ up to 21 June 2022, $0.121\text{ }^{\circ}\text{C}$ on or after 22 June 2022)



c) CSIRO (mean difference: $0.069\text{ }^{\circ}\text{C}$, standard deviation of difference: $0.159\text{ }^{\circ}\text{C}$)



d) RAL (mean difference: $-0.060\text{ }^{\circ}\text{C}$, standard deviation of difference: $0.073\text{ }^{\circ}\text{C}$)

Figure 14 Agreement with reference value (continued on next page)

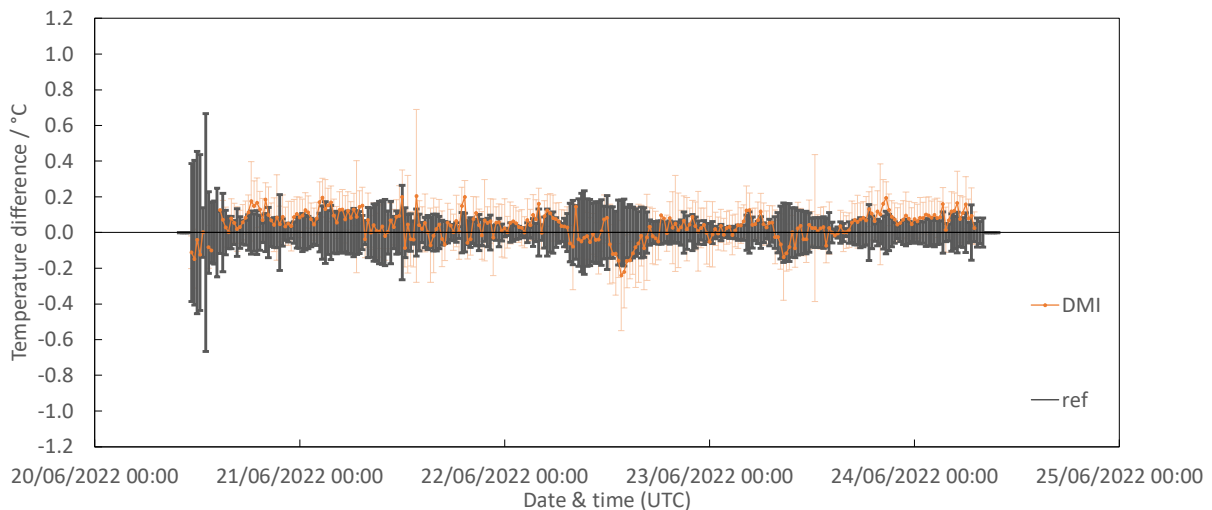
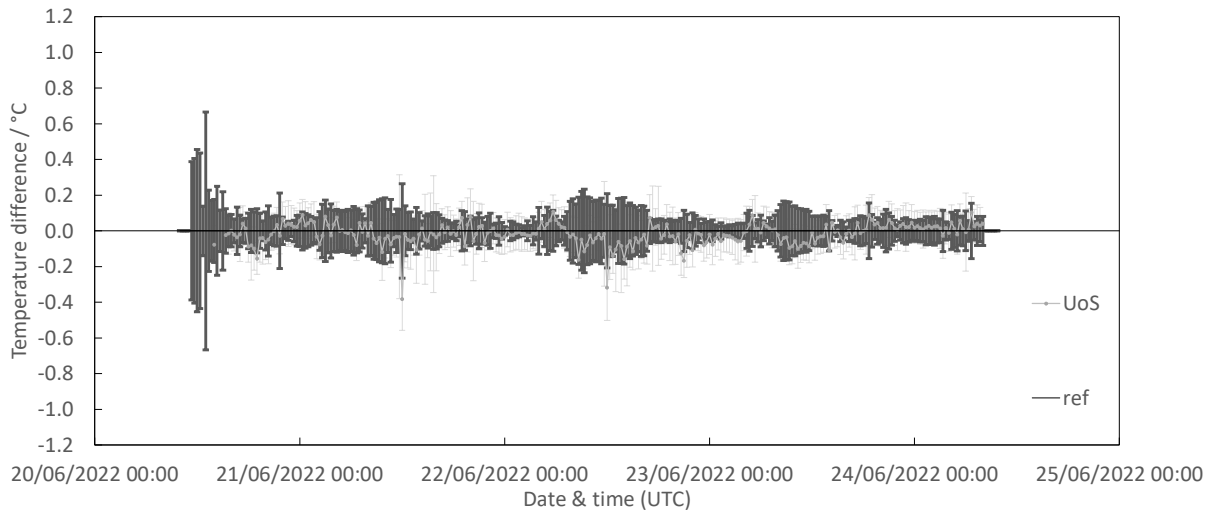


Figure 14 Agreement with reference value (cont.)

Error bars are, respectively, the expanded uncertainty ($k = 2$) of the participant measurement and of the reference value

7 DISCUSSIONS

The SSTs measured by the participants (see group photo in Fig. 15), shown in Fig. 12 a), all show the daily rise and fall of the temperature, with the highest temperature varying about 2 °C depending on the day. The reference temperature during the 5-day period was in the range from 16.8 °C to 19.8 °C , so the comparison was able to cover this 3.0 °C temperature range, which is approximately two times larger than the previous comparison at a water reservoir [7].



Figure 15 Comparison participants

The agreement among all participants is relatively good initially on the 20 and 21 June. However, as mentioned in the previous section, an abrupt shift in the KIT value occurred just before midnight of the 21, whereafter the offset of around $-0.4\text{ }^{\circ}\text{C}$ remain. The pilot later notified KIT of this irregularity, but nothing could be found by KIT upon reviewing the measurement data that can explain the abrupt change in behaviour, and so no change was made to the data. The shift is seen in the sea brightness temperature (Fig. 12 d)) but not in the sky brightness temperature (Fig. 12 e)). Two separate radiometers are used for the two measurements by KIT, so it appears that the radiometer measuring the sea was affected.

It is also noticeable in Fig. 12 a) that the scatter of the SST measurement by CSIRO (plotted in yellow) was large until the afternoon of the 20 June, when it suddenly decreased and stayed small thereafter. A closer inspection reveals that this is seen in both the sea surface brightness temperature and the sky brightness temperature, which is expected because for the ISAR the same radiometer measures both temperatures. Upon notification from the pilot after submission of data, CSIRO investigated the cause but could not find any clue to what might have caused this and thus the result stays as it is. A possible explanation is some noise through the power line was present in the beginning but somehow disappeared afterwards. The scatter does not influence the measurement in a systematic way and is taken into account in the slightly larger measurement uncertainty for this period as shown in Fig. 14 c).

In the sky brightness temperature data of Fig. 12 e), each day just before noon except for the 23 June, a spike is seen for measurements by DMI, RAL, CSIRO and UoS. KIT data do not show this phenomenon. UoV submitted data after eliminating this part of data. The spike is thought to be caused by the light from the sun coming into the field of view of the radiometer when measuring the sky brightness temperature: the pier is extending towards the south with a slight tilt to the east, and the radiometers were all aligned straight out, and considering the

geolocation of Bournemouth which is to the west of Greenwich, all seem to indicate the cause to be the sun coming in view just before noon. This did not happen on the 23 June, for the sun was behind the clouds. KIT had a different orientation from the others for its sky viewing radiometer. The effect of the spike in the sky brightness measurement results in a slight dip in the SST corrected for the reflection, and this is visible in Fig. 12 a), but this is short and hardly noticeable except for the spikes seen in Figs. 12 c) and 14 a) for UoV around noon for two days, and has insignificant effect on the overall result of the comparison.

The scatter of the participants' measured SST over time was evaluated in Fig. 13 a). As seen from the plot, the scatter becomes largest around or before noon each day. The ambient temperature and humidity are plotted in b) of the same figure, and the ISAR internal BB temperature in c), as possible influencing factors. The increase and decrease in the scatter in a) seem to show a similar trend as the rise and fall of the ambient temperature (b)). However, it is hard to explain why the scatter becomes large when the SST and the ambient temperature become closer, since in the nighttime, ambient temperature falls much lower than the SST while in the daytime the two are relatively close. If, on the other hand, one compares a) with c) which is absolute difference of the average of the internal BB temperature of the three ISAR instruments from the ambient temperature, we notice that they have very similar temporal trend, and the daytime temperature of the internal BB gets to be two to five degrees higher than the SST. It is understandable that the ISAR and the SISTeR both utilising the internal BB, will have larger scatter in their measurements when the SST and the internal BB temperature deviates, which shows up as the increase in scatter during daytime in Fig. 13 a). UoV's CIMEL radiometer also utilises an internal cavity structure for the same purpose [10].

Figure 12 e) shows the sky brightness temperature which is representative of the cloud condition: it is low when it is sunny, and high when there is cloud. If we compare Fig. 12 e) with Fig. 13 a), we do not see any relation between the two, indicating that the correction for the reflected sky radiance is working well. It should be noted that this is when the emissivity values adopted were not exactly the same for all participants. A variation of approximately 0.005 in emissivity would lead to approximately 0.23 °C variation on a clear day and approximately 0.07 °C with overcast cloud in the correction for emissivity, which indicates that the participants adopted emissivity values that represent each one's measurement conditions appropriately.

The error bars in Fig. 14, one for the participant measurement and the other for the reference value, represent the expanded uncertainty for $k = 2$. Overlap of the two error bars means the agreement of the measurement with the reference. All participants show good agreement throughout the five-day comparison period, the only exception being a slight deviation by KIT for a short period after the unexplained abrupt shift on the 21 June just before midnight.

The mean of the difference from the reference value is shown for each participant in Fig. 14. With the exception of KIT on or after 22 June, all values are within ± 0.07 °C. This is more than two times improvement when compared to the previous comparison in 2016 for the same six participants [7]. The improvement is striking if one takes into account the two times wider temperature range of comparison. The reason for the improvement is not clear, although it can most likely be attributed to the good measurement conditions and careful undertaking by the participants. Compared to the last comparison at an inland water reservoir, in this comparison the participants were all able to view the sea facing south in order to avoid shadows. Favourable weather conditions with fewer clouds and less precipitation could also have contributed. Good mixing of the water by tide and wave may have played a role. The observed sea surface was clear of any obstacles at all times.

The uncertainty of the comparison reference value is around 0.1 °C ($k = 2$). The participant measurement uncertainty ranges from roughly 0.1 °C to 0.75 °C ($k = 2$). Therefore, the reference value uncertainty is small enough and the comparison accurate enough to verify the agreement of participant radiometers. It should be noted that the agreement evidenced here

is with the mean of the participant measurements. This means the comparison only supports agreement among the participants when measuring SST (even though the uncertainties reported by participants include calibration uncertainty). There is a possibility of a systematic offset in the reference value due to systematic offsets in the measurement and calibration of the radiometers involved, which is the subject of investigation in the two laboratory-based comparisons of the CRIC, where direct comparisons are made against NPL reference standards [AD-4, AD-5].

8 CONCLUSIONS

SST measurement capabilities of six participating institutes were evaluated through a comparison of radiometers at Boscombe Pier, Bournemouth, on the south coast of England as a part of the CEOS International Thermal Infrared Radiometer Inter-comparison (CRIC). During the comparison which took place during five days in June 2022, the six radiometers viewed the sea surface from the tip of the pier and the measured temperatures were compared after correcting for emissivity and reflected radiation from the sky.

All participants' reported values agreed with the reference value within the uncertainties. Here, the reference value was evaluated as the simple mean of the participant measured SSTs. The mean of the difference from the reference value taken over the whole comparison period was evaluated for each participant and all were found to be within 0.07 °C, which is half of what was reported in the previous comparison in 2016 [7].

Although the measured SST range was about 3 °C, which is two times wider than the previous comparison, it is still limited when considering the actual SST that one needs to measure in the ocean. It will be of interest to conduct a similar comparison at a different location or during a different season to cover a wider or different temperature range.

An issue that became apparent was an abrupt shift in one of the radiometers: the reading shifted by -0.4 °C from the middle of the comparison period for an undetermined reason, and data after this shift was excluded from the comparison. The shift is quite obvious when comparison is made with other radiometers, but if no other radiometers are around, it would be extremely difficult to detect. When the radiometer is deployed onboard a ship, even if one detects there was a shift through a recalibration after return from the trip, it will be impossible to identify whether the shift was abrupt or gradual, or when it had happened. The radiometers in the current comparison have internal BB or cavity sources to track and correct for any drifts, some with two high-precision internal blackbodies. The result of the current comparison confirms the importance of such systems.

It was unfortunate that the number of participants was smaller than the last comparison primarily due to travel restrictions imposed by the COVID-19 pandemic. In recent years, new improved radiometers for SST measurements are being developed, and more radiometers are being deployed at the sea. A future repeat of the current exercise will be needed, possibly with a reduced interval between comparisons than the current six to eight years, when the new radiometers are being used in the field.

References

- [1] Barton, I. J., Minnett, P. J., Maillet K. A., Donlon, C. J., Hook, S. J., Jessup, A. T. and Nightingale, T.J. (2004) "The Miami 2001 infrared radiometer calibration and intercomparison: Part II Shipboard results", *J. Atmos. Ocean Techn.*, 21, 268-283.
- [2] Rice, J. P., Butler, J. I., Johnson, B. C., Minnett, P. J., Maillet K. A., Nightingale, T. J, Hook, S. J., Abtahi, A., Donlon, C. J. and Barton, I. J. (2004) "The Miami 2001 infrared radiometer calibration and intercomparison. Part I: Laboratory characterisation of blackbody targets", *J. Atmos. Ocean Techn.*, 21, 258-267.

- [3] Theocharous, E. and Fox, N. P. (2010) “CEOS comparison of IR brightness temperature measurements in support of satellite validation. Part II: Laboratory comparison of the brightness temperature of blackbodies”, *NPL Report COM OP4*.
- [4] Theocharous, E., Usadi, E. and Fox, N. P. (2010) “CEOS comparison of IR brightness temperature measurements in support of satellite validation. Part I: Laboratory and ocean surface temperature comparison of radiation thermometers”, *NPL Report COM OP3*.
- [5] Theocharous, E., Barker Snook, I. and Fox, N. P. (2017) “2016 comparison of IR brightness temperature measurements in support of satellite validation. Part 1: Laboratory comparison of the brightness temperature of blackbodies”, *NPL Report ENV 12*.
- [6] Theocharous, E., Barker Snook, I. and Fox, N. P. (2017) “2016 comparison of IR brightness temperature measurements in support of satellite validation. Part 2: Laboratory comparison of radiation thermometers”, *NPL Report ENV 14*.
- [7] Theocharous, E., Barker Snook, I. and Fox, N. P. (2017) “2016 comparison of IR brightness temperature measurements in support of satellite validation. Part 3: Sea surface temperature comparison of radiation thermometers”, *NPL Report ENV 15*.
- [8] Theocharous, E., Fox, N. P., Barker-Snook, I., Niclòs, R., García-Santos, V., Minnett, P. J., Göttsche, F. M., Poutier, L., Morgan, N., Nightingale, T., Wimmer, W., Høyer, J., Zhang, K., Yang, M., Guan, L., Arbelo, M. and Donlon, C. J. (2019) “The 2016 CEOS infrared radiometer comparison: Part 2: Laboratory comparison of radiation thermometers”, *J. Atmos. Ocean Techn.*, 36, 1079-1092.
- [9] Sicard, M., Spyak, P. R., Brogniez, G., Legrand, M., Abuhassan, N. K., Pietras, C., and Buis, J. P. (1999). “Thermal infrared field radiometer for vicarious cross-calibration: characterization and comparisons with other field instruments”, *Optical Engineering*, 38 (2), 345-356.
- [10] Legrand, M., Pietras, C., Brogniez, G., Haeffelin, M., Abuhassan, N. K. and Sicard, M. (2000). “A high-accuracy multiwavelength radiometer for in situ measurements in the thermal infrared. Part I: characterization of the instrument”, *J. Atmos. Ocean Techn.*, 17, 1203-1214.
- [11] Coll, C., Niclòs, R., Puchades, J., García-Santos, V., Galve, J.M., Pérez-Planells, L., Valor, E., Theocharous, E. (2019) “Laboratory calibration and field measurement of land surface temperature and emissivity using thermal infrared multiband radiometers”, *Int. J. Appl. Earth Obs. Geoinformation*, 78, 227-239.
- [12] Niclòs, R., Caselles, V., Valor, E., Coll, C. and Sanchez, J. M. (2009). A simple equation for determining the sea surface emissivity in the 3–15 μm region. *Int. J. Remote Sens.*, vol. 30, no. 6, pp. 1603–1619.
- [13] Wu, X. and Smith, W.L. (1997). Emissivity of rough sea surface for 8-13 μm : modelling and verification. *Applied Optics*, 36: 2609-2619.
- [14] Salisbury, J. W. and D’Aria, D. M. (1992). Emissivity of terrestrial materials in the 8-14 micrometer atmospheric window. *Remote Sensing of Environment*, 42, 83-106.
- [15] Niclòs, R., and Caselles, V. (2008). Water salinity and foam coverage effects on thermalinfrared sea surface emissivity. In: *Ocean Remote Sensing: Recent Techniques and Applications*: 111-131. Research Singpost. ISBN: 978-81-308-0268-8.
- [16] Niclos, R., Valor, E., Caselles, V., Coll, C., and Sanchez, J.M. (2005). In situ angular measurements of thermal infrared sea surface emissivity – Validation of models. *Remote Sensing of Environment*, 94: 83-93.
- [17] Niclos, R., Doña; C., Valor, E., & Bisquert, M. (2014). Thermal-Infrared Spectral and Angular Characterization of Crude Oil and Seawater Emissivities for Oil Slick Identification. *IEEE Transactions on Geoscience and Remote Sensing*, Vol. 52 (9), 5387- 5395.

- [18] Niclos, R., Caselles, V., Coll, C., Valor, E., and Rubio, E. (2004). Autonomous Measurements of Sea Surface Temperature Using In Situ Thermal Infrared Data. *Journal of Atmospheric and Oceanic Technology*, 21: 683-692.
- [19] Barton, I. J., A. M. Zavody, D. M. O'Brien, D. R. Cutten, R. W. Saunders, and D. T. Llewelling-Jones (1989), Theoretical algorithms for satellite-derived sea surface temperatures, *J. Geophys. Res.*, 94, 3365– 3375.
- [20] Niclòs, R., Caselles, V., Valor, E., and Coll, C. (2007). Foam effect on the sea surface emissivity in the 8–14 μm region. *Journal of Geophysical Research – Oceans*, 112, Issue C12.
- [21] Martí-Cardona, B., Prats, J., Niclòs, R. (2021), Enhancing the retrieval of stream surface temperature from Landsat data, *Remote Sensing of Environment*, 224: 182-191.
- [22] Niclòs, R., Valiente, J.A., Barberà, M.J., Coll, C. (2015). An Autonomous System to Take Angular Thermal-Infrared Measurements for Validating Satellite Products. *Remote Sensing*, 7, 15269-15294.
- [23] Niclòs, R., Pérez-Planells, Ll., Coll, C., Valiente, J.A., Valor, E. (2018) Evaluation of the S-NPP VIIRS land surface temperature product using ground data acquired by an autonomous system at a rice paddy. *ISPRS J. Photogramm. Remote Sens.*, 135, 1-12.
- [24] Niclòs, R., Puchades, J., Coll, C., Barberà, M.J., Pérez-Planells, L., Valiente, J.A., Sánchez, J.M. (2021). Evaluation of Landsat-8 TIRS data recalibrations and land surface temperature split-window algorithms over a homogeneous crop area with different phenological land covers. *ISPRS J. Photogramm. Remote Sens.*, 174: 237-253.
- [25] Donlon, C., Robinson, I. S., Wimmer, W., Fisher, G., Reynolds, M., Edwards, R., & Nightingale, T. J. (2008) “An infrared sea surface temperature autonomous radiometer (ISAR) for deployment aboard volunteer observing ships (VOS)”. *J. Atmos. Ocean Techn.*, 25, 93-113.
- [26] Wimmer, W., and Robinson, I. (2016) “The ISAR instrument uncertainty model”, *J. Atmos. Ocean Techn.*, 33, 2415-2433
- [27] Donlon, C., Wimmer, W., Robinson, I. S., Fisher, G., Ferlet, M., Nightingale, T. J. and Bras, B. (2014) “A Second-Generation Blackbody System for the Calibration and Verification of Seagoing Infrared Radiometers”, *J. Atmos. Ocean Techn.*, 31, 1104-1127
- [28] http://www.atsr.rl.ac.uk/validation/sister/sis_inst/index.shtml